Abstract: Different nonlinear optical interactions in a novel SRS-active non-centrosymmetric tetragonal crystal $Ca_2ZnSi_2O_7$ were investigated at room and cryogenic (≈ 9 K) temperature under picosecond laser pumping. In addition to measuring octave-spanning Stokes and anti-Stokes combs we observed several cascaded and cross-cascaded $\chi^{(3)} \leftrightarrow \chi^{(3)}$ effects involving several SRS-active phonons. All recorded Raman-induced lasing lines in the visible and near-IR range are identified and attributed to the SRS-promoting vibration transitions. A brief review of SRS- and Nd^{3+}-doped laser-active melilite-type crystals is given as well.

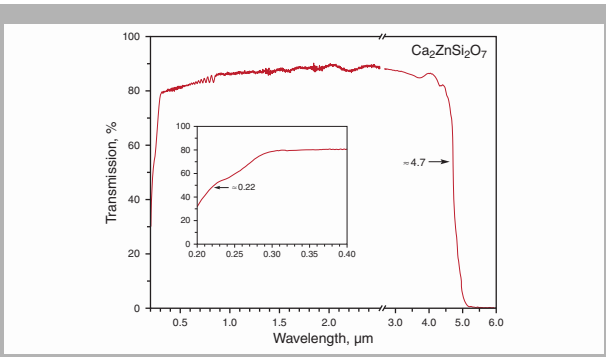

Transmission spectrum of a crystal of tetragonal $Ca_2ZnSi_2O_7$, recorded at room temperature using a (100) plate of ≈ 1.33 mm thickness

Many-phonon stimulated Raman scattering and related cascaded and cross-cascaded $\chi^{(3)}$-nonlinear optical effects in melilite-type crystal $Ca_2ZnSi_2O_7$

A.A. Kaminskii, [1,*] *H. Rhee,* [2] *O. Lux,* [2] *H.J. Eichler,* [2] *L. Bohatý,* [3,*] *P. Becker,* [3] *J. Liebertz,* [3] *K. Ueda,* [4] *A. Shirakawa,* [4] *V.V. Koltashev,* [5] *J. Hanuza,* [6,7] *J. Dong,* [8] *and D.B. Stavrovskii* [9]

[1] Institute of Crystallography, Russian Academy of Sciences, Moscow 119333, Russia
[2] Institute of Optics and Atomic Physics, Technical University of Berlin, 10623 Berlin, Germany
[3] Institute of Crystallography, University of Cologne, 50939 Cologne, Germany
[4] Institute for Laser Science, University of Electro-Communications, 182-8585 Tokyo, Japan
[5] Fiber Optical Research Center, Russian Academy of Sciences, Moscow 119333, Russia
[6] Institute of Low Temperature and Structure Research, Polish Academy of Sciences, Wrocław 50950, Poland
[7] Department of Bioorganic Chemistry, Institute of Chemistry and Food Technology, Wrocław University of Economics, Wrocław 50345, Poland
[8] Department of Electronics Engineering, Xiamen University, Xiamen 361005, China
[9] Institute of General Physics, Russian Academy of Sciences, Moscow 119333, Russia

Received: 18 June 2011, Revised: Accepted: 21 June 2011
Published online: 29 September 2011

Key words: non-centrosymmetric crystal; $Ca_2ZnSi_2O_7$; hardystonite; Raman crystal; many-phonon stimulated Raman scattering; SRS; SHG; THG; Stokes and anti-Stokes lasing comb; combined SRS-active phonons; cascaded and cross-cascaded self-frequency generation; Raman laser shifter

1. Introduction

For more than forty years, beginning with [1], the laser (with Ln^{3+} ions) and nonlinear-optical properties of non-centrosymmetric tetragonal melilite-type crystals are in the focus of attention of many groups of researchers (see, e.g. [2–8]). Special attention in recent years was devoted to studies of various manifestation of cascaded $\chi^{(3)} \leftrightarrow \chi^{(3)}$ and $\chi^{(3)} \leftrightarrow \chi^{(2)}$ interactions in these crystals and to elici-

* Corresponding author: e-mail: kaminalex@mail.ru, ladislav.bohaty@uni-koeln.de

Crystal	SE channels of Nd^{3+} ions	Observed $\chi^{(3)}$- and $\chi^{(2)}$-nonlinear laser effects	SRS-promoting vibration modes, cm^{-1}
$Ca_2ZnSi_2O_7$ [a]		**SRS, SHG** [b], **THG** [c], **self-SFG(SRS)** [d], **St-ASt comb** [e], [**present work**]	**≈906**, **≈663**, **≈614**, **≈243** [f] [**present work**]
$Ca_2Ga_2SiO_7$	$^4F_{3/2} \rightarrow {}^4I_{11/2}$ [13–15] $^4F_{3/2} \rightarrow {}^4I_{13/2}$ [3,15]	**SRS**, **self-SFG(SRS)** [**present work**] [g]	**≈667**, **≈500** [**present work**]
$Sr_2MgGe_2O_7$		SRS, SHG, THG, SFG, self-SFG(FD) [h], self-SFG(FD,SRS) [i], St-ASt comb [12]	≈779 [12]
$Sr_2ZnGe_2O_7$		SRS, SHG, THG, SFG, self-SFG(FD), self-SFG(FD,SRS), St-ASt comb [11]	≈778 [11]
$Ba_2MgGe_2O_7$	$^4F_{3/2} \rightarrow {}^4I_{11/2}$ [1,5]	SRS, SHG, THG, SFG, "Cherenkov-type" SHG [j], self-FD(SRS) [k], self-SRS(FD) [l], self-SRS(SFG) [m], self-SFG(FD,SRS) [n], St-ASt comb [9]	771.5 [9]
$Ba_2ZnGe_2O_7$	$^4F_{3/2} \rightarrow {}^4I_{11/2}$ [2,5]	SRS, SHG, THG, SFG, self-FD(SRS), self-SRS(FD), self-SRS(SRS), St-ASt comb [12]	≈770, ≈257 [12]

Note: only references from peer-reviewed journals are included.
[a] Also known as mineral hardystonite (see, e.g. [16]). [b] SHG: the second harmonic generation. [c] THG: the third harmonic generation.
[d] Self-SFG(SRS): the sum-frequency generation, i.e. SFG from pump radiation and its Stokes and anti-Stokes components.
[e] St-ASt comb: Stokes and anti-Stokes multi-wavelength comb lasing.
[f] At ≈9 K the energy of SRS-promoting modes were measured: ≈920, ≈670, ≈620, ≈250, and ≈300 cm^{-1}. The latter two are combined modes and occur as results of the interaction of the first three $\chi^{(3)}$-active vibrations of studied crystal.
[g] These data are highly preliminary, given with the aim to indicate in this "review" table that $Ca_2Ga_2SiO_7$ doped with Nd^{3+} lasants also acts as a SRS-active crystal.
[h] Self-SFG(FD): the self-sum-frequency generation, i.e. SFG from the arising Stokes and anti-Stokes components of pumping radiation.
[i] Self-SFG(FD,SRS): the self-sum-frequency generation, i.e. SFG from the arising SHG and components of Stokes and anti-Stokes generation.
[j] "Cherenkov-type" SHG: the conical harmonic generation *via* Cherenkov-type effects can occur in cases where the propagation velocity of the generated nonlinear polarization wave in a bulk crystal is higher than the phase velocities of the arising harmonic wavelengths. In such cases the polarization wave, propagating with the group velocity v_f of the fundamental wavelength in a crystal with normal dispersion of refractive indices, generates harmonics, which interfere constructively by fulfilling the Cherenkov-type condition at a conical angle α (*versus* the wave normal of the fundamental wavelength), where α is given by $\cos\alpha = v_{SHG(THG)}/v_f$. This results in intense SHG or THG on the envelope of a cone.
[k] Self-FD(SRS): the self-frequency doubling, i.e., SHG from the arising SRS lasing components.
[l] Self-SRS(FD): SRS from the arising SHG of the pumping wave or of other lasing radiation.
[m] Self-SRS(SFG): SRS from the arising intense SFG of the pumping wavelength and further lasing radiation.
[n] Self-SFG(FD,SRS): the self-sum-frequency generation, i.e. SFG from the arising SHG and components of Stokes and anti-Stokes generation.

Table 1 Selected SRS- and SE-active (with Nd^{3+} lasants) active synthetic crystals with the melilite-type structure

Property				
Space group of averaged structure [a] [16,22]	$D_{2d}^3 - P\bar{4}2_1m$ (No.113)			
Unit cell parameters of averaged structure, Å [18]	$a = b = 7.8279(10)$; $c = 5.0138(6)$			
Site symmetry (SS) and coordination number (CN) of atoms in the averaged structure [18]		SS	CN	Wyckoff letter
	Ca	$m(C_s)$	8	(4e)
	Zn	$\bar{4}(S_4)$	4	(2a)
	Si	$m(C_s)$	4	(4e)
	O1	$2mm(C_{2v})$		(2c)
	O2	$m(C_s)$		(4e)
	O3	$1(C_1)$		(8f)
Formula units per unit cell [18]	$Z = 2$			
Nonlinearities	$\chi^{(2)} + \chi^{(3)}$			
Optical transparency, cm^{-1} [b]	≈0.22 – ≈4.7 (see Fig. 1)			
Linear optical character [19]	Uniaxial negative ($n_o > n_e$)			
Phonon spectra extension, cm^{-1} [c]	≈1050			
Energy of SRS promoting vibration modes, cm^{-1} [d]	$\omega_{SRS1} \approx 906$; $\omega_{SRS2} \approx 663$; $\omega_{SRS3} \approx 614$; $\omega_{SRS4} \approx 243$			
FWHM linewidth for the Raman shifted lines, related to SRS-promoting modes, cm^{-1}	$\Delta\nu_{R1} \approx 11$; $\Delta\nu_{R2} \approx 13$; $\Delta\nu_{R3} \approx 11$			
Steady-state Raman gain coefficient for the first Stokes lasing component, cm/GW	$g_{ssR}^{St_{1-1}} \geq 0.2$ (for $\lambda_{St1-1} = 1.1777$ μm)			

[a] At room temperature, $Ca_2ZnSi_2O_7$ shows a two-dimensionally incommensurately modulated crystal structure, the normal melilite-type structure occurs above ca. 405 K (e.g. [22]).
[b] For a polished (100) plate of ≈ 1.33 mm thickness.
[c] From spontaneous Raman scattering and IR absorption spectra.
[d] At ≈ 9 K we observed five SRS-promoting vibration modes (see Table 1).

Table 2 Some physical properties of tetragonal crystal $Ca_2ZnSi_2O_7$ at room temperature

Pumping condition		$\chi^{(3)}$- and $\chi^{(2)}$-nonlinear lasing components			SRS-promoting vibration modes, cm^{-1}			
λ_f, μm	Excitation geometry [a]	Wavelength, μm [b]	Lasing line [c]	Attribution [d]	ω_{SRS1}	ω_{SRS2}	ω_{SRS3}	ω_{SRS4} [e]
0.53207	$\mathbf{e}_1[\mathbf{e}_3\mathbf{e}_3]\mathbf{e}_1$ see Fig. 3b	0.4649	ASt_{3-1}	$\omega_{f2}+3\omega_{SRS1}=$ $=[\omega_{f2}+(\omega_{f2}+2\omega_{SRS1})-(\omega_{f2}-\omega_{SRS1})]=$ $=[\omega_{f2}+\omega_{ASt2-1}-\omega_{St1-1}]=\omega_{ASt3-1}$	≈ 906			
		0.4853	ASt_{2-1}	$\omega_{f2}+2\omega_{SRS1}=$ $=[\omega_{f2}+(\omega_{f2}+\omega_{SRS1})-(\omega_{f2}-\omega_{SRS1})]=$ $=[\omega_{f2}+\omega_{ASt1-1}-\omega_{St1-1}]=\omega_{ASt2-1}$	≈ 906			
		0.5076	ASt_{1-1}	$\omega_{f2}+\omega_{SRS1}=$ $=[\omega_{f2}+\omega_{f2}-(\omega_{f2}-\omega_{SRS1})]=$ $=[\omega_{f2}+\omega_{f2}-\omega_{St1-1}]=\omega_{ASt1-1}$	≈ 906			
		0.53207	λ_{f2}	ω_{f2}	–	–	–	–
		0.5590	St_{1-1}	$\omega_{f2}-\omega_{SRS1}=\omega_{St1-1}$	≈ 906			
		0.5889	St_{2-1}	$\omega_{f2}-2\omega_{SRS1}=[(\omega_{f2}-\omega_{SRS1})-\omega_{SRS1}]=$ $=[\omega_{St1-1}-\omega_{SRS1}]=\omega_{St2-1}$	≈ 906			
1.06415	$\mathbf{e}_3[\mathbf{e}_1\mathbf{e}_1]\mathbf{e}_3$ see Fig. 4a	0.3547	THG-SFG$\{\lambda_{f1}\}$	$[\omega_{SHG}+(\omega_{SHG}-\omega_{f1})]=\omega_{THG}$	–	–	–	–
		0.5076	self-SFG$\{\lambda_{f1},\lambda_{ASt1-1}\}$	$[\omega_{f1}+(\omega_{f1}+\omega_{SRS1})]=\omega_{SHG}+\omega_{SRS1}=$ $=\omega_{SFG,ASt1-1}$	≈ 906			
		0.53207	SHG$\{\lambda_{f1}\}$	$\omega_{f1}+\omega_{f1}=\omega_{SHG}$	≈ 906			
		0.5590	self-SFG$\{\lambda_{f1},\lambda_{St1-1}\}$	$[\omega_{f1}+(\omega_{f1}-\omega_{SRS1})]=\omega_{SHG}-\omega_{SRS1}=$ $=\omega_{SFG,St1-1}$	≈ 906			
	$\mathbf{e}_1[\mathbf{e}_3\mathbf{e}_3]\mathbf{e}_1$ see Fig. 4b	0.3437	self-SFG$\{\lambda_{f1},\lambda_{ASt1-1}\}$	$[\omega_{f1}+\omega_{f1}+\omega_{ASt1-1}]=$ $=[\omega_{f1}+\omega_{f1}+(\omega_{f1}+\omega_{SRS1})]=$ $=\omega_{THG}+\omega_{SRS1}=\omega_{SFG,ASt1-1}$	≈ 906			
		0.3547	THG$\{\lambda_{f1}\}$	$\omega_{f1}+\omega_{f1}+\omega_{f1}=\omega_{THG}$	–	–	–	–
		0.3665	self-SFG$\{\lambda_{f1},\lambda_{St1-1}\}$	$[\omega_{f1}+\omega_{f1}+\omega_{St1-1}]=$ $=[\omega_{f1}+\omega_{f1}+(\omega_{f1}-\omega_{SRS1})]=$ $=\omega_{THG}-\omega_{SRS1}=\omega_{SFG,St1-1}$	≈ 906			
		0.3791	self-SFG$\{\lambda_{f1},\lambda_{St2-1}\}$	$[\omega_{f1}+\omega_{f1}+\omega_{St2-1}]=$ $=[\omega_{f1}+\omega_{f1}+(\omega_{f1}-2\omega_{SRS1})]=$ $=\omega_{THG}-2\omega_{SRS1}=\omega_{SFG,St2-1}$	≈ 906			
		0.3926	self-SFG$\{\lambda_{f1},\lambda_{St3-1}\}$	$[\omega_{f1}+\omega_{f1}+\omega_{St3-1}]=$ $=[\omega_{f1}+\omega_{f1}+(\omega_{f1}-3\omega_{SRS1})]=$ $=\omega_{THG}-3\omega_{SRS1}=\omega_{SFG,St3-1}$	≈ 906			
		0.4070 [f]	self-SFG$\{\lambda_{f1},\lambda_{St4-1}\}$	$[\omega_{f1}+\omega_{f1}+\omega_{St4-1}]=$ $=[\omega_{f1}+\omega_{f1}+(\omega_{f1}-4\omega_{SRS1})]=$ $=\omega_{THG}-4\omega_{SRS1}=\omega_{SFG,St4-1}$	≈ 906			
		0.5164	ASt_{11-1}	$\omega_{f1}+11\omega_{SRS1}=$ $=[\omega_{f1}+(\omega_{f1}+10\omega_{SRS1})-(\omega_{f1}-\omega_{SRS1})]=$ $=[\omega_{f1}+\omega_{ASt10-1}-\omega_{St1-1}]=\omega_{ASt11-1}$	≈ 906			
		0.5418	ASt_{10-1}	$\omega_{f1}+10\omega_{SRS1}=$ $=[\omega_{f1}+(\omega_{f1}+9\omega_{SRS1})-(\omega_{f1}-\omega_{SRS1})]=$ $=[\omega_{f1}+\omega_{ASt9-1}-\omega_{St1-1}]=\omega_{ASt10-1}$	≈ 906			
		0.5698	ASt_{9-1}	$\omega_{f1}+9\omega_{SRS1}=$ $=[\omega_{f1}+(\omega_{f1}+8\omega_{SRS1})-(\omega_{f1}-\omega_{SRS1})]=$ $=[\omega_{f1}+\omega_{ASt8-1}-\omega_{St1-1}]=\omega_{ASt9-1}$	≈ 906			
		0.6008	ASt_{8-1}	$\omega_{f1}+8\omega_{SRS1}=$ $=[\omega_{f1}+(\omega_{f1}+7\omega_{SRS1})-(\omega_{f1}-\omega_{SRS1})]=$ $=[\omega_{f1}+\omega_{ASt7-1}-\omega_{St1-1}]=\omega_{ASt8-1}$	≈ 906			
		0.6354	ASt_{7-1}	$\omega_{f1}+7\omega_{SRS1}=$ $[\omega_{f1}+(\omega_{f1}+6\omega_{SRS1})-(\omega_{f1}-\omega_{SRS1})]=$ $=[\omega_{f1}+\omega_{ASt6-1}-\omega_{St1-1}]=\omega_{AS7-1}$	≈ 906			

		0.6742	ASt_{6-1}	$\omega_{f1}+6\omega_{SRS1}=$ $=[\omega_{f1}+(\omega_{f1}+5\omega_{SRS1})-(\omega_{f1}-\omega_{SRS1})]=$ $=[\omega_{f1}+\omega_{ASt5-1}-\omega_{St1-1}]=\omega_{ASt6-1}$	≈906			
		0.7180	ASt_{5-1}	$\omega_{f1}+5\omega_{SRS1}=$ $=[\omega_{f1}+(\omega_{f1}+4\omega_{SRS1})-(\omega_{f1}-\omega_{SRS1})]=$ $=[\omega_{f1}+\omega_{ASt4-1}-\omega_{St1-1}]=\omega_{ASt5-1}$	≈906			
	see Fig. 4c, Fig. 4d	0.6008	ASt_{8-1}	$\omega_{f1}+8\omega_{SRS1}=$ $=[\omega_{f1}+(\omega_{f1}+7\omega_{SRS1})-(\omega_{f1}-\omega_{SRS1})]=$ $=[\omega_{f1}+\omega_{ASt7-1}-\omega_{St1-1}]=\omega_{ASt8-1}$	≈906			
		0.6354	ASt_{7-1}	$\omega_{f1}+7\omega_{SRS1}=$ $=[\omega_{f1}+(\omega_{f1}+6\omega_{SRS1})-(\omega_{f1}-\omega_{SRS1})]=$ $=[\omega_{f1}+\omega_{ASt6-1}-\omega_{St1-1}]=\omega_{AS7-1}$	≈906			
		0.6742	ASt_{6-1}	$\omega_{f1}+6\omega_{SRS1}=$ $=[\omega_{f1}+(\omega_{f1}+5\omega_{SRS1})-(\omega_{f1}-\omega_{SRS1})]=$ $=[\omega_{f1}+\omega_{ASt5-1}-\omega_{St1-1}]=\omega_{ASt6-1}$	≈906			
		0.7180	ASt_{5-1}	$\omega_{f1}+5\omega_{SRS1}=$ $=[\omega_{f1}+(\omega_{f1}+4\omega_{SRS1})-(\omega_{f1}-\omega_{SRS1})]=$ $=[\omega_{f1}+\omega_{ASt4-1}-\omega_{St1-1}]=\omega_{ASt5-1}$	≈906			
		0.7680	ASt_{4-1}	$\omega_{f1}+4\omega_{SRS1}=$ $=[\omega_{f1}+(\omega_{f1}+3\omega_{SRS1})-(\omega_{f1}-\omega_{SRS1})]=$ $=[\omega_{f1}+\omega_{ASt3-1}-\omega_{St1-1}]=\omega_{ASt4-1}$	≈906			
		0.8254	ASt_{3-1}	$\omega_{f1}+3\omega_{SRS1}=$ $=[\omega_{f1}+(\omega_{f1}+2\omega_{SRS1})-(\omega_{f1}-\omega_{SRS1})]=$ $=[\omega_{f1}+\omega_{ASt2-1}-\omega_{St1-1}]=\omega_{ASt3-1}$	≈906			
		0.8921	ASt_{2-1}	$\omega_{f1}+2\omega_{SRS1}=$ $=[\omega_{f1}+(\omega_{f1}+\omega_{SRS1})-(\omega_{f1}-\omega_{SRS1})]=$ $=[\omega_{f1}+\omega_{ASt1-1}-\omega_{St1-1}]=\omega_{ASt2-1}$	≈906			
		0.9706	ASt_{1-1}	$\omega_{f1}+\omega_{SRS1}=$ $=[\omega_{f1}+\omega_{f1}-(\omega_{f1}-\omega_{SRS1})]=$ $=[\omega_{f1}+\omega_{f1}-\omega_{St1-1}]=\omega_{ASt1-1}$	≈906			
		0.9940	ASt_{1-2}	$\omega_{f1}+\omega_{SRS2}=$ $=[\omega_{f1}+\omega_{f1}-(\omega_{f1}-\omega_{SRS2})]=$ $=[\omega_{f1}+\omega_{f1}-\omega_{St1-2}]=\omega_{ASt1-2}$		≈663		
		1.06415	λ_{f1}	ω_{f1}	–	–	–	–
		1.1449	St_{1-2}	$\omega_{f1}-\omega_{SRS2}=\omega_{St1-2}$		≈663		
		1.1777	St_{1-1}	$\omega_{f1}-\omega_{SRS1}=\omega_{St1-1}$	≈906			
		1.2775	$St_{1-2}\{St_{1-1}\}$	$[(\omega_{f1}-\omega_{SRS1})-\omega_{SRS2}]=$ $=\omega_{St1-1}-\omega_{SRS2}=\omega_{St1-2\{St1-1\}}$	≈906	≈663		
		1.3184	St_{2-1}	$\omega_{f1}-2\omega_{SRS1}=$ $=[(\omega_{f1}-\omega_{SRS1})-\omega_{SRS1}]=$ $=[\omega_{St1-1}-\omega_{SRS1}]=\omega_{St2-1}$	≈906			
		1.4972	St_{3-1}	$\omega_{f1}-3\omega_{SRS1}=$ $=[(\omega_{f1}-2\omega_{SRS1})-\omega_{SRS1}]=$ $=[\omega_{St2-1}-\omega_{SRS1}]=\omega_{St3-1}$	≈906			
		1.7322 [f)]	St_{4-1}	$\omega_{f1}-4\omega_{SRS1}=$ $=[(\omega_{f1}-3\omega_{SRS1})-\omega_{SRS1}]=$ $=[\omega_{St3-1}-\omega_{SRS1}]=\omega_{St4-1}$	≈906			
0.53207	$\mathbf{e}_2[(\mathbf{e}_1+\mathbf{e}_3)(\mathbf{e}_1+\mathbf{e}_3)]\mathbf{e}_2$ see Fig. 5a	0.4523	ASt_{5-2}	$\omega_{f2}+5\omega_{SRS2}=$ $=[\omega_{f2}+(\omega_{f2}+4\omega_{SRS2})-(\omega_{f2}-\omega_{SRS2})]=$ $=[\omega_{f2}+\omega_{ASt4-2}-\omega_{St1-2}]=\omega_{ASt5-2}$		≈663		
		0.4663	ASt_{4-2}	$\omega_{f2}+4\omega_{SRS2}=$ $=[\omega_{f2}+(\omega_{f2}+3\omega_{SRS2})-(\omega_{f2}-\omega_{SRS2})]=$ $=[\omega_{f2}+\omega_{ASt3-2}-\omega_{St1-2}]=\omega_{ASt4-2}$		≈663		
		0.4812	ASt_{3-2}	$\omega_{f2}+3\omega_{SRS2}=$ $=[\omega_{f2}+(\omega_{f2}+2\omega_{SRS2})-(\omega_{f2}-\omega_{SRS2})]=$ $=[\omega_{f2}+\omega_{ASt2-2}-\omega_{St1-2}]=\omega_{ASt3-2}$		≈663		

		0.4970	ASt_{2-2}	$\omega_{f2}+2\omega_{SRS2}=$ $=[\omega_{f2}+(\omega_{f2}+\omega_{SRS2})-(\omega_{f2}-\omega_{SRS2})]=$ $=[\omega_{f2}+\omega_{ASt1-2}-\omega_{St1-2}]=\omega_{ASt2-2}$		≈ 663		
		0.5139	ASt_{1-2}	$\omega_{f2}+\omega_{SRS2}=$ $=[(\omega_{f2}+\omega_{f2}-(\omega_{f2}-\omega_{SRS2})]=$ $=[(\omega_{f2}+\omega_{f2})-(\omega_{St1-2}]=\omega_{ASt1-2}$		≈ 663		
		0.5152	ASt_{1-3}	$\omega_{f2}+\omega_{SRS3}=$ $=[(\omega_{f2}+\omega_{f2})-(\omega_{f2}-\omega_{SRS3})]=$ $=[(\omega_{f2}+\omega_{f2})-(\omega_{St1-3}]=\omega_{ASt1-3}$			≈ 614	
		0.53207	λ_{f2}	ω_{f2}	–	–	–	–
		0.5500	St_{1-3}	$\omega_{f2}-\omega_{SRS3}=\omega_{St1-3}$			≈ 614	
		0.5515	St_{1-2}	$\omega_{f2}-\omega_{SRS2}=\omega_{St1-2}$		≈ 663		
		0.5590	St_{1-1}	$\omega_{f2}-\omega_{SRS1}=\omega_{St1-1}$	≈ 906			
		0.5725	St_{2-2}	$\omega_{f2}-2\omega_{SRS2}=[(\omega_{f2}-\omega_{SRS2})-\omega_{SRS2}]=$ $=[(\omega_{St1-2}-\omega_{SRS2}]=\omega_{St2-2}$		≈ 663		
		0.5951	St_{3-2}	$\omega_{f2}-3\omega_{SRS2}=$ $=[(\omega_{f2}-2\omega_{SRS2})-\omega_{SRS2}]=$ $=[(\omega_{St2-2}-\omega_{SRS2}]=\omega_{St3-2}$		≈ 663		
	$\mathbf{e}_1[(\mathbf{e}_2+\mathbf{e}_3)$ $(\mathbf{e}_2+\mathbf{e}_3)]\mathbf{e}_1$ see Fig. 5b	0.4461	ASt_{4-1}	$\omega_{f2}+4\omega_{SRS1}=$ $=[\omega_{f2}+(\omega_{f2}+3\omega_{SRS1})-(\omega_{f2}-\omega_{SRS1})]=$ $=[\omega_{f2}+\omega_{ASt3-1}-\omega_{St1-1}]=\omega_{ASt4-1}$	≈ 906			
		0.4649	ASt_{3-1}	$\omega_{f2}+3\omega_{SRS1}=$ $=[\omega_{f2}+(\omega_{f2}+2\omega_{SRS1})-(\omega_{f2}-\omega_{SRS1})]=$ $=[\omega_{f2}+\omega_{ASt2-1}-\omega_{St1-1}]=\omega_{ASt3-1}$	≈ 906			
		0.4812	ASt_{3-2}	$\omega_{f2}+3\omega_{SRS2}=$ $=[\omega_{f2}+(\omega_{f2}+2\omega_{SRS2})-(\omega_{f2}-\omega_{SRS2})]=$ $=[\omega_{f2}+\omega_{ASt2-2}-\omega_{St1-2}]=\omega_{ASt3-2}$		≈ 663		
		0.4853	ASt_{2-1}	$\omega_{f2}+2\omega_{SRS1}=$ $=[\omega_{f2}+(\omega_{f2}+\omega_{SRS1})-(\omega_{f2}-\omega_{SRS1})]=$ $=[\omega_{f2}+\omega_{ASt1-1}-\omega_{St1-1}]=\omega_{ASt2-1}$	≈ 906			
		0.4911	$ASt_{1-2}\{ASt_{1-1}\}$	$[(\omega_{f2}+\omega_{SRS1})+\omega_{SRS2}]=$ $=\omega_{ASt1-2\{ASt1-1\}}$	≈ 906	≈ 663		
		0.4970	ASt_{2-2}	$\omega_{f2}+2\omega_{SRS2}=$ $=[\omega_{f2}+(\omega_{f2}+\omega_{SRS2})-(\omega_{f2}-\omega_{SRS2})]=$ $=[\omega_{f2}+\omega_{ASt1-2}-\omega_{St1-2}]=\omega_{ASt2-2}$		≈ 663		
		0.5014	$ASt_{1-4}\{ASt_{1-1}\}$	$[(\omega_{f2}+\omega_{SRS1})+\omega_{SRS4}]=$ $=\omega_{ASt1-4\{ASt1-1\}}$	≈ 906			≈ 243
		0.5076	ASt_{1-1}	$\omega_{f2}+\omega_{SRS1}=$ $=[\omega_{f2}+\omega_{f2}-(\omega_{f2}-\omega_{SRS1})]=$ $=[\omega_{f2}+\omega_{f2}-\omega_{St1-1}]=\omega_{ASt1-1}$	≈ 906			
		0.5139	ASt_{1-2}	$\omega_{f2}+\omega_{SRS2}=$ $=[(\omega_{f2}+\omega_{f2}-(\omega_{f2}-\omega_{SRS2})]=$ $=[\omega_{f2}+\omega_{f2}-\omega_{St1-2}]=\omega_{ASt1-2}$		≈ 663		
		0.5152	ASt_{1-3}	$\omega_{f2}+\omega_{SRS3}=$ $=[(\omega_{f2}+\omega_{f2}-(\omega_{f2}-\omega_{SRS3})]=$ $=[\omega_{f2}+\omega_{f2}-\omega_{St1-3}]=\omega_{ASt1-3}$			≈ 614	
		0.5253	ASt_{1-4}	$\omega_{f2}+\omega_{SRS4}=$ $=[(\omega_{f2}+\omega_{f2}-(\omega_{f2}-\omega_{SRS4})]=$ $=[\omega_{f2}+\omega_{f2}-\omega_{St1-4}]=\omega_{ASt1-4}$				≈ 243
		0.53297	λ_{f2}	ω_{f2}	–	–	–	–
		0.5390	St_{1-4}	$\omega_{f2}-\omega_{SRS4}=\omega_{St1-4}$				≈ 243
		0.5500	St_{1-3}	$\omega_{f2}-\omega_{SRS3}=\omega_{St1-3}$			≈ 614	
		0.5515	St_{1-2}	$\omega_{f2}-\omega_{SRS2}=\omega_{St1-2}$		≈ 663		
		0.5590	St_{1-1}	$\omega_{f2}-\omega_{SRS1}=\omega_{St1-1}$	≈ 906			
		0.5667	$St_{1-4}\{St_{1-1}\}$	$[(\omega_{f2}-\omega_{SRS1})-\omega_{SRS4}]=$ $=\omega_{St1-4\{St1-1\}}$	≈ 906			≈ 243

		0.5725	St_{2-2}	$\omega_{f2}-2\omega_{SRS2}=[(\omega_{f2}-\omega_{SRS2})-\omega_{SRS2}]=$ $=[(\omega_{St1-2}-\omega_{SRS2}]=\omega_{St2-2}$		≈ 663		
		0.5805	$St_{1-2}\{St_{1-1}\}$	$[(\omega_{f2}-\omega_{SRS1})-\omega_{St1-2}]=$ $=\omega_{St1-2\{St1-1\}}$	≈ 906	≈ 663		
		0.5889	St_{2-1}	$\omega_{f2}-2\omega_{SRS1}=[(\omega_{f2}-\omega_{SRS1})-\omega_{SRS1}]=$ $=[\omega_{St1-1}-\omega_{SRS1}]=\omega_{St2-1}$	≈ 906			
1.06415	$\mathbf{e}_2[\mathbf{e}_3\mathbf{e}_3]\mathbf{e}_2$ see Fig. 6a	0.3437	self-SFG$\{\lambda_{f1},\lambda_{ASt1-1}\}$	$[\omega_{f1}+\omega_{f1}+\omega_{ASt1-1}]=$ $=[\omega_{f1}+\omega_{f1}+(\omega_{f1}+\omega_{SRS1})]=$ $=\omega_{THG}+\omega_{SRS1}=\omega_{SFG,ASt1-1}$	≈ 906			
		0.3547	THG$\{\lambda_{f1}\}$	$\omega_{f1}+\omega_{f1}+\omega_{f1}=\omega_{THG}$	≈ 906			
		0.3665	self-SFG$\{\lambda_{f1},\lambda_{St1-1}\}$	$[\omega_{f1}+\omega_{f1}+\omega_{St1-1}]=$ $=[\omega_{f1}+\omega_{f1}+(\omega_{f1}-\omega_{SRS1})]=$ $=\omega_{THG}-\omega_{SRS1}=\omega_{SFG,St1-1}$	≈ 906			
		0.3791	self-SFG$\{\lambda_{f1},\lambda_{St2-1}\}$	$[\omega_{f1}+\omega_{f1}+\omega_{St2-1}]=$ $=[\omega_{f1}+\omega_{f1}+(\omega_{f1}-2\omega_{SRS1})]=$ $=\omega_{THG}-2\omega_{SRS1}=\omega_{SFG,St2-1}$	≈ 906			
		0.3926	self-SFG$\{\lambda_{f1},\lambda_{St3-1}\}$	$[\omega_{f1}+\omega_{f1}+\omega_{St3-1}]=$ $=[\omega_{f1}+\omega_{f1}+(\omega_{f1}-3\omega_{SRS1})]=$ $=\omega_{THG}-3\omega_{SRS1}=\omega_{SFG,St3-1}$	≈ 906			
		0.5418	ASt_{10-1}	$\omega_{f1}+10\omega_{SRS1}=$ $=[\omega_{f1}+(\omega_{f1}+9\omega_{SRS1})-(\omega_{f1}-\omega_{SRS1})]=$ $=[\omega_{f1}+\omega_{ASt9-1}-\omega_{St1-1}]=\omega_{ASt10-1}$	≈ 906			
		0.5698	ASt_{9-1}	$\omega_{f1}+9\omega_{SRS1}=$ $=[\omega_{f1}+(\omega_{f1}+8\omega_{SRS1})-(\omega_{f1}-\omega_{SRS1})]=$ $=[\omega_{f1}+\omega_{ASt8-1}-\omega_{St1-1}]=\omega_{ASt9-1}$	≈ 906			
		0.6008	ASt_{8-1}	$\omega_{f1}+8\omega_{SRS1}=$ $=[\omega_{f1}+(\omega_{f1}+7\omega_{SRS1})-(\omega_{f1}-\omega_{SRS1})]=$ $=[\omega_{f1}+\omega_{ASt7-1}-\omega_{St1-1}]=\omega_{ASt8-1}$	≈ 906			
	$\mathbf{e}_2[\mathbf{e}_3\mathbf{e}_3]\mathbf{e}_2$ see Fig. 6b, Fig. 6c	0.6354	ASt_{7-1}	$\omega_{f1}+7\omega_{SRS1}=$ $=[\omega_{f1}+(\omega_{f1}+6\omega_{SRS1})-(\omega_{f1}-\omega_{SRS1})]=$ $=[\omega_{f1}+\omega_{ASt6-1}-\omega_{St1-1}]=\omega_{AS7-1}$	≈ 906			
		0.6742	ASt_{6-1}	$\omega_{f1}+6\omega_{SRS1}=$ $=[\omega_{f1}+(\omega_{f1}+5\omega_{SRS1})-(\omega_{f1}-\omega_{SRS1})]=$ $=[\omega_{f1}+\omega_{ASt5-1}-\omega_{St1-1}]=\omega_{ASt6-1}$	≈ 906			
		0.6854	$ASt_{1-2}\{ASt_{5-1}\}$	$[(\omega_{f1}+5\omega_{SRS1})+\omega_{SRS2}]=$ $=[\omega_{ASt5-1}+\omega_{SRS2}]=\omega_{ASt1-2\{ASt5-1\}}$	≈ 906	≈ 663		
		0.7057	$St_{1-2}\{ASt_{6-1}\}$	$[(\omega_{f1}+6\omega_{SRS1})-\omega_{SRS2}]=$ $=[\omega_{ASt6-1}-\omega_{SRS2}]=\omega_{St1-2\{ASt6-1\}}$	≈ 906	≈ 663		
		0.7180	ASt_{5-1}	$\omega_{f1}+5\omega_{SRS1}=$ $=[\omega_{f1}+(\omega_{f1}+4\omega_{SRS1})-(\omega_{f1}-\omega_{SRS1})]=$ $=[\omega_{f1}+\omega_{ASt4-1}-\omega_{St1-1}]=\omega_{ASt5-1}$	≈ 906			
		0.7308	$ASt_{1-2}\{ASt_{4-1}\}$	$[(\omega_{f1}+4\omega_{SRS1})+\omega_{SRS2}]=$ $=[\omega_{ASt4-1}+\omega_{SRS2}]=\omega_{ASt1-2\{ASt4-1\}}$	≈ 906	≈ 663		
		0.7539	$St_{1-2}\{ASt_{5-1}\}$	$[(\omega_{f1}+5\omega_{SRS1})-\omega_{SRS2}]=$ $=[\omega_{ASt5-1}-\omega_{SRS2}]=\omega_{St1-2\{ASt5-1\}}$	≈ 906	≈ 663		
		0.7680	ASt_{4-1}	$\omega_{f1}+4\omega_{SRS1}=$ $=[\omega_{f1}+(\omega_{f1}+3\omega_{SRS1})-(\omega_{f1}-\omega_{SRS1})]=$ $=[\omega_{f1}+\omega_{ASt3-1}-\omega_{St1-1}]=\omega_{ASt4-1}$	≈ 906			
		0.7826	$ASt_{1-2}\{ASt_{3-1}\}$	$[(\omega_{f1}+3\omega_{SRS1})+\omega_{SRS2}]=$ $=[\omega_{ASt3-1}+\omega_{SRS2}]=\omega_{ASt1-2\{ASt3-1\}}$	≈ 906	≈ 663		
		0.8092	$St_{1-2}\{ASt_{4-1}\}$	$[(\omega_{f1}+4\omega_{SRS1})-\omega_{SRS2}]=$ $=[\omega_{ASt4-1}-\omega_{SRS2}]=\omega_{St1-2\{ASt4-1\}}$	≈ 906	≈ 663		
		0.8254	ASt_{3-1}	$\omega_{f1}+3\omega_{SRS1}=$ $=[\omega_{f1}+(\omega_{f1}+2\omega_{SRS1})-(\omega_{f1}-\omega_{SRS1})]=$ $=[\omega_{f1}+\omega_{ASt2-1}-\omega_{St1-1}]=\omega_{ASt3-1}$	≈ 906			

		0.8423	$ASt_{1-2}\{ASt_{2-1}\}$	$[(\omega_{f1}+2\omega_{SRS1})+\omega_{SRS2}]=$ $=[\omega_{ASt2-1}+\omega_{SRS2}]=\omega_{ASt1-2\{ASt2-1\}}$	≈ 906	≈ 663		
		0.8732	$St_{1-2}\{ASt_{3-1}\}$	$[(\omega_{f1}+3\omega_{SRS1})-\omega_{SRS2}]=$ $=[\omega_{ASt3-1}-\omega_{SRS2}]=\omega_{St1-2\{ASt3-1\}}$	≈ 906	≈ 663		
		0.8921	ASt_{2-1}	$\omega_{f1}+2\omega_{SRS1}=$ $=[\omega_{f1}+(\omega_{f1}+\omega_{SRS1})-(\omega_{f1}-\omega_{SRS1})]=$ $=[\omega_{f1}+\omega_{ASt1-1}-\omega_{St1-1}]=\omega_{ASt2-1}$	≈ 906			
		0.9119	$ASt_{1-2}\{ASt_{1-1}\}$	$[(\omega_{f1}+\omega_{SRS1})+\omega_{SRS2}]=$ $=[\omega_{ASt1-1}+\omega_{SRS2}]=\omega_{ASt1-2\{ASt1-1\}}$	≈ 906	≈ 663		
		0.9482	$St_{1-2}\{ASt_{2-1}\}$	$[(\omega_{f1}+2\omega_{SRS1})-\omega_{SRS2}]=$ $=[\omega_{ASt2-1}-\omega_{SRS2}]=\omega_{St1-2\{ASt2-1\}}$	≈ 906	≈ 663		
		0.9706	ASt_{1-1}	$\omega_{f1}+\omega_{SRS1}=$ $=[\omega_{f1}+\omega_{f1}-(\omega_{f1}-\omega_{SRS1})]=$ $=[\omega_{f1}+\omega_{f1}-\omega_{St1-1}]=\omega_{ASt1-1}$	≈ 906			
		0.9940	ASt_{1-2}	$\omega_{f1}+\omega_{SRS2}=$ $=[\omega_{f1}+\omega_{f1}-(\omega_{f1}-\omega_{SRS2})]=$ $=[\omega_{f1}+\omega_{f1}-\omega_{St1-2}]=\omega_{ASt1-2}$		≈ 663		
		0.9989	ASt_{1-3}	$\omega_{f1}+\omega_{SRS3}=$ $=[\omega_{f1}+\omega_{f1}-(\omega_{f1}-\omega_{SRS3})]=$ $=[\omega_{f1}+\omega_{f1}-\omega_{St1-3}]=\omega_{ASt1-3}$			≈ 614	
		1.06415	λ_{f1}	ω_{f1}	–	–	–	–
		1.1386	St_{1-3}	$\omega_{f1}-\omega_{SRS3}=\omega_{St1-3}$			≈ 614	
		1.1449	St_{1-2}	$\omega_{f1}-\omega_{SRS2}=\omega_{St1-2}$		≈ 663		
		1.1777	St_{1-1}	$\omega_{f1}-\omega_{SRS1}=\omega_{St1-1}$	≈ 906			
		1.2124	$ASt_{1-2}\{St_{2-1}\}$	$[(\omega_{f1}-2\omega_{SRS1})+\omega_{SRS2}]=$ $=[\omega_{St2-1}+\omega_{SRS2}]=\omega_{ASt1-2\{St2-1\}}$	≈ 906	≈ 663		
		1.2775	$St_{1-2}\{St_{1-1}\}$	$[(\omega_{f1}-\omega_{SRS1})-\omega_{SRS2}]=$ $=[\omega_{St1-1}-\omega_{SRS2}]=\omega_{St1-2\{ASt2-1\}}$	≈ 906	≈ 663		
		1.3184	St_{2-1}	$\omega_{f1}-2\omega_{SRS1}=$ $=[(\omega_{f1}-\omega_{SRS1})-\omega_{SRS1}]=$ $=[\omega_{St1-1}-\omega_{SRS1}]=\omega_{St2-1}$	≈ 906			
		1.4972	St_{3-1}	$\omega_{f1}-3\omega_{SRS1}=$ $=[(\omega_{f1}-2\omega_{SRS1})-\omega_{SRS1}]=$ $=[\omega_{St2-1}-\omega_{SRS1}]=\omega_{St3-1}$	≈ 906			

[a] Notation is used in analogy to [28]. The characters between square brackets are (from left to right): the polarization direction of the pump wave and the nonlinear laser generation, respectively, while the characters to the left and to right of the square brackets are the direction of the wave normals of the pump wave and of the generated nonlinear-laser components, respectively.

[b] Measurement accuracy is ± 0.0003 μm.

[c] THG-SFG: the cascaded third harmonic generation arising *via* parametric four-wave mixing under collinear coherent pumping at fundamental pump radiation at $\lambda_{f1} = 1.06415$ μm wavelength and its SHG. THG$\{\lambda_{f1}\}$: the third harmonic generation *via* $\chi^{(3)}$-nonlinear interaction. SHG$\{\lambda_{f1}\}$: the second harmonic generation *via* $\chi^{(2)}$-nonlinear interaction. Self-SFG$\{\lambda_{f1},\lambda_{ASt1-1}\}$: the cascaded sum-frequency generation arising from one-micron fundamental pump radiation at $\lambda_{f1} = 1.06415$ μm wavelength and its first Stokes nonlinear-laser generation. $ASt_{1-4}\{ASt_{1-1}\}$: the Raman-induced four-wave mixing (RFWM) of the first anti-Stokes component related to the "$\chi^{(3)}$-active combined vibration mode $\omega_{SRS1-4} \approx 243$ cm^{-1} by the cross-cascaded lasing which arising from the first anti-Stokes component related to the first original SRS-promoting vibration mode $\omega_{SRS1-1} \approx 906$ cm^{-1} of the crystal. $St_{1-2}\{St_{1-1}\}$: the first Stokes component related to the second original vibration mode $\omega_{SRS2} \approx 663$ cm^{-1} generated by the cross-cascaded lasing from the first Stokes component related to the first original SRS promoting vibration mode $\omega_{SRS1-1} \approx 906$ cm^{-1} of the crystal.

[d] In square brackets, the most probable nonlinear-laser components of the SRS or RFWM processes are given.

[e] The "masked" SRS-active vibration arising in the nonlinear $\chi^{(3)}$-interaction of the two original promoting vibration modes $\omega_{SRS1} \approx 906$ cm^{-1} and $\omega_{SRS3} \approx 663$ cm^{-1} (see also text).

[f] Due to the "zero" sensitivity of our InGaAs-CCD detector (see Fig. 2b), we could not register a signal at the fourth Stokes wavelength at $\lambda_{St4-1} = 1.7322$ μm under one-micron pumping, but its probable presence is indicated by the detected signal at a wavelength of 0.4070 μm, which we have attributed as the parametric process of frequency summing $[\omega_{f1}+\omega_{f1}+\omega_{St4-1}]=[\omega_{f1}+\omega_{f1}+(\omega_{f1}-4\omega_{SRS1})]=\omega_{THG}-4\omega_{SRS1}=\omega_{SFG,St4-1}$.

Table 3 Spectral composition of SRS and RFWM generation, as well as of cascaded $\chi^{(3)} \leftrightarrow \chi^{(2)}$ and cross-cascaded $\chi^{(3)} \leftrightarrow \chi^{(2)}$ nonlinear lasing in the crystal of $Ca_2ZnSi_2O_7$, recorded at room temperature with picosecond Nd^{3+}:$Y_3Al_5O_{12}$-laser pumping at two fundamental wavelengths $\lambda_{f1} = 1.06415$ μm and $\lambda_{f2} = 0.53207$ μm

Pumping condition	$\chi^{(3)}$-lasing components			SRS-promoting vibration modes, cm^{-1}				
Excitation geometry	Wavelength, μm	Lasing line	Attribution	ω_{SRS1}	ω_{SRS2}	ω_{SRS3}	ω_{SRS4}	ω_{SRS5}
$\mathbf{e}_1[\mathbf{e}_3\mathbf{e}_3]\mathbf{e}_1$ see Fig. 3a	0.4639	AST_{3-1}	$\omega_{f2}+3\omega_{SRS1}=$ $=[\omega_{f2}+(\omega_{f2}+2\omega_{SRS1})-(\omega_{f2}-\omega_{SRS1})]=$ $=[\omega_{f2}+\omega_{ASt2-1}-\omega_{St1-1}]=\omega_{ASt3-1}$	≈ 920				
	0.4846	AST_{2-1}	$\omega_{f2}+2\omega_{SRS1}=$ $=[\omega_{f2}+(\omega_{f2}+\omega_{SRS1})-(\omega_{f2}-\omega_{SRS1})]=$ $=[\omega_{f2}+\omega_{ASt1-1}-\omega_{St1-1}]=\omega_{ASt2-1}$	≈ 920				
	0.5072	AST_{1-1}	$\omega_{f2}+\omega_{SRS1}=[\omega_{f2}+\omega_{f2}-(\omega_{f2}-\omega_{SRS1})]=$ $=[\omega_{f2}+\omega_{f2}-\omega_{St1-1}]=\omega_{ASt1-1}$	≈ 920				
	0.53207	λ_{f2}	ω_{f2}	–	–	–	–	–
	0.5595	St_{1-1}	$\omega_{f2}-\omega_{SRS1}=\omega_{St1-1}$	≈ 920				
	0.5898	St_{2-1}	$\omega_{f2}-2\omega_{SRS1}=[(\omega_{f2}-\omega_{SRS1})-\omega_{SRS1}]=$ $=[\omega_{St1-1}-\omega_{SRS1}]=\omega_{St2-1}$	≈ 920				
	0.6237	St_{3-1}	$\omega_{f2}-3\omega_{SRS1}=[(\omega_{f2}-2\omega_{SRS1})-\omega_{SRS1}]=$ $=[\omega_{St2-1}-\omega_{SRS1}]=\omega_{St3-1}$	≈ 920				
$\mathbf{e}_1[(\mathbf{e}_2+\mathbf{e}_3)(\mathbf{e}_2+\mathbf{e}_3)]\mathbf{e}_1$ see Fig. 7	0.4846	AST_{2-1}	$\omega_{f2}+2\omega_{SRS1}=$ $[\omega_{f2}+(\omega_{f2}+\omega_{SRS1})-(\omega_{f2}-\omega_{SRS1})]=$ $=[\omega_{f2}+\omega_{ASt1-1}-\omega_{St1-1}]=\omega_{ASt2-1}$	≈ 920				
	0.4906	$AST_{1-2}\{AST_{1-1}\}$	$[(\omega_{f2}+\omega_{SRS1})+\omega_{SRS2}]=\omega_{ASt1-2\{ASt1-1\}}$	≈ 920	≈ 670			
	0.4918	$AST_{1-3}\{AST_{1-1}\}$	$[(\omega_{f2}+\omega_{SRS1})+\omega_{SRS3}]=\omega_{ASt1-3\{ASt1-1\}}$	≈ 920		≈ 620		
	0.4996	$AST_{1-5}\{AST_{1-1}\}$	$[(\omega_{f2}+\omega_{SRS1})+\omega_{SRS5}]=\omega_{ASt1-5\{ASt1-1\}}$	≈ 920				≈ 300
	0.5009	$AST_{1-4}\{AST_{1-1}\}$	$[(\omega_{f2}+\omega_{SRS1})+\omega_{SRS4}]=\omega_{ASt1-4\{ASt1-1\}}$	≈ 920			≈ 250	
	0.5072	AST_{1-1}	$\omega_{f2}+\omega_{SRS1}=[\omega_{f2}+\omega_{f2}-(\omega_{f2}-\omega_{SRS1})]=$ $=[\omega_{f2}+\omega_{f2}-\omega_{St1-1}]=\omega_{ASt1-1}$	≈ 920				
	0.5138	AST_{1-2}	$\omega_{f2}+\omega_{SRS2}=[(\omega_{f2}+\omega_{f2}-(\omega_{f2}-\omega_{SRS2})]=$ $=[\omega_{f2}+\omega_{f2}-\omega_{St1-2}]=\omega_{ASt1-2}$		≈ 670			
	0.5151	AST_{1-3}	$\omega_{f2}+\omega_{SRS3}=[(\omega_{f2}+\omega_{f2}-(\omega_{f2}-\omega_{SRS3})]=$ $=[\omega_{f2}+\omega_{f2}-\omega_{St1-3}]=\omega_{ASt1-3}$			≈ 620		
	0.5237	AST_{1-5}	$\omega_{f2}+\omega_{SRS5}=[(\omega_{f2}+\omega_{f2}-(\omega_{f2}-\omega_{SRS5})]=$ $=[\omega_{f2}+\omega_{f2}-\omega_{St1-5}]=\omega_{ASt1-5}$					≈ 300
	0.5251	AST_{1-4}	$\omega_{f2}+\omega_{SRS4}=[(\omega_{f2}+\omega_{f2}-(\omega_{f2}-\omega_{SRS4})]=$ $=[\omega_{f2}+\omega_{f2}-\omega_{St1-4}]=\omega_{ASt1-4}$				≈ 250	
	0.53207	λ_{f2}	ω_{f2}	–	–	–	–	–
	0.5392	St_{1-4}	$\omega_{f2}-\omega_{SRS4}=\omega_{St1-4}$				≈ 250	
	0.5407	St_{1-5}	$\omega_{f2}-\omega_{SRS5}=\omega_{St1-5}$					≈ 300
	0.5502	St_{1-3}	$\omega_{f2}-\omega_{SRS3}=\omega_{St1-3}$			≈ 620		
	0.5517	St_{1-2}	$\omega_{f2}-\omega_{SRS2}=\omega_{St1-2}$		≈ 670			
	0.5595	St_{1-1}	$\omega_{f2}-\omega_{SRS1}=\omega_{St1-1}$	≈ 920				
	0.5674	$St_{1-4}\{St_{1-1}\}$	$[(\omega_{f2}-\omega_{SRS1})-\omega_{SRS4}]=\omega_{St1-4\{St1-1\}}$	≈ 920			≈ 250	
	0.5690	$St_{1-5}\{St_{1-1}\}$	$[(\omega_{f2}-\omega_{SRS1})-\omega_{SRS5}]=\omega_{St1-5\{St1-1\}}$	≈ 920				≈ 300
	0.5796	$St_{1-3}\{St_{1-1}\}$	$[(\omega_{f2}-\omega_{SRS1})-\omega_{St3}=\omega_{St1-3\{St1-1\}}$	≈ 920		≈ 620		
	0.5813	$St_{1-2}\{St_{1-1}\}$	$[(\omega_{f2}-\omega_{SRS1})-\omega_{St2}=\omega_{St1-2\{St1-1\}}$	≈ 920	≈ 670			
	0.5898	St_{2-1}	$\omega_{f2}-2\omega_{SRS1}=[(\omega_{f2}-\omega_{SRS1})-\omega_{SRS1}]=$ $=[\omega_{St1-1}-\omega_{SRS1}]=\omega_{St2-1}$	≈ 920				

Note: all explanations and notations are as in Table 3.

Table 4 Spectral composition of SRS and RFWM generation, as well as cascaded and cross-cascaded $\chi^{(3)} \leftrightarrow \chi^{(3)}$ nonlinear lasing in the crystal of $Ca_2ZnSi_2O_7$, recorded at ≈ 9 K with picosecond Nd^{3+}:$Y_3Al_5O_{12}$-laser pumping at fundamental wavelength $\lambda_{f2} = 0.53207$ μm (SHG)

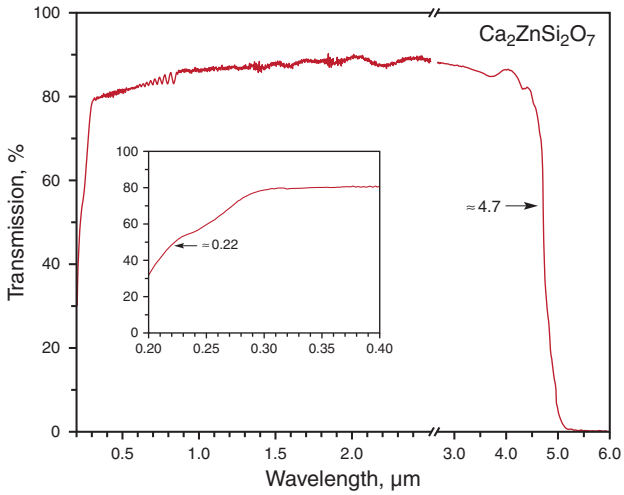

Figure 1 (online color at www.lphys.org) Transmission spectrum of a crystal of tetragonal $Ca_2ZnSi_2O_7$, recorded at room temperature using a (100) plate of ≈ 1.33 mm thickness. The wavelength range of UV, visible and near-IR was recorded with spectrophotometer Perkin Elmer (model Lambda 19 UV/VIS/NIR) the mid-IR part with a spectrophotometer Bruker (model Vector-22). The estimation of the UV (see inset) and mid-IR borders of the optical transmission at 50% transmission level (given in μm) are indicated by arrows

Vibration mode, cm^{-1} [a]	Tentative assignment [b]
60 w	$T'(Si_2O_7)+T'(Zn^{2+})+T'(Ca^{2+})$
100 m	$T'(Zn^{2+})+T'(Ca^{2+})$
115 w	
145 vw	
220 w	$\rho(SiO_3)+T'(Ca^{2+})$
240 w	$\delta(SiOSi)+\delta_{as}(SiO_3)$
265 w	
445 m	$\delta_{as}(SiO_3)+\delta(SiOSi)$
480 m	
550 w	$\delta_{as}(SiO_3)$
614 s	$\delta_s(SiO_3)+\delta_s(SiOSi)$
663 vs	$\nu_s(SiOSi)+\nu_s(SiO_3)$
906 vs	$\nu_s(SiO_3)$
1020 vw	$\nu_{as}(SiOSi)$
1060 m	

Notation: s – strong, vs – very strong, m – medium, w – weak, vw – very weak. Bold numerals indicate the vibration modes that promote SRS lasing in $Ca_2ZnSi_2O_7$ crystals

[a] Measurement accuracy ± 2 cm^{-1}.

[b] It will be clarified in a forthcoming article on the polarized spontaneous Raman scattering and IR spectra.

Table 5 Band wavenumbers of the first order room-temperature spontaneous Raman scattering A_1-spectrum (see Fig. 8) of a tetragonal $Ca_2ZnSi_2O_7$ single crystal

tation of their nonlinear-optical potential to generate multi-octave Stokes and anti-Stokes combs, as well as to the determination the nature of their vibration modes responsible for the effect of stimulated Raman scattering (SRS) [9–12]. As follows from Table 1, in addition to this work SRS generation and other manifestations of $\chi^{(3)}$-nonlinear laser interactions were discovered and studied only in four crystals of the large family of melilite-type crystals. This table indicates that some of them being activated by Nd^{3+} ions show laser activity. Below are the results of our SRS-experiments with the melilite-type crystal $Ca_2ZnSi_2O_7$ with respect to spectroscopic investigations of its $\chi^{(3)}$-nonlinear optical properties under picosecond laser excitation in the visible and near-IR region at room and cryogenic (≈ 9 K) temperature.

2. Stokes and anti-Stokes lasing

Investigations of the different manifestations of Raman induced frequency generation based on $\chi^{(3)}$- and $\chi^{(2)}$-nonlinearities in tetragonal $Ca_2ZnSi_2O_7$ single crystals were carried out in the single-pass (cavity free) excitation geometry scheme using an experimental setup that was described already in our earlier experiments on SRS-spectroscopy of four other isotypic melilite-type crystals $Sr_2MgGe_2O_7$, $Sr_2ZnGe_2O_7$, $Ba_2MgGe_2O_7$, and $Ba_2ZnGe_2O_7$ (see Table 1). Unlike in previous room-temperature $\chi^{(3)}$-lasing investigations with germanium melilites, in the present work it was necessary to conduct experiments at cryogenic temperature because the studied crystal exhibits several SRS-promoting vibration modes which are not fully manifested at room-temperature measurements due to overlapping of several of its $\chi^{(3)}$-lasing lines. However, we are aware that the possibility of a phase transition from incommensurately modulated phase of $Ca_2ZnSi_2O_7$ (at room temperature) into a commensurate lock-in phase at low temperatures [17] or into a different modulated phase [22] is still under debate. Several selected physical properties of $Ca_2ZnSi_2O_7$ single crystal relevant to our research are given in Table 2. Other known properties can be found in (see e.g. [16–27]). In the present work all the basic experiments on SRS-spectroscopy were performed with oriented and polished samples prepared from single crystals of $Ca_2ZnSi_2O_7$ that were grown in the Institute of Crystallography of the University of Cologne. The samples were of parallel-epipedal shape with faces $\{110\}$ and $\{001\}$. Faces were polished but without antireflection coating. The results given in Table 3 and Table 4 (corresponding to Fig. 3 – Fig. 7) were obtained with a sample of dimensions 10.18 mm $\| \mathbf{e}_1$, 13.54 mm $\| \mathbf{e}_2$, and 15.83 mm $\| \mathbf{e}_3$, with

$$\mathbf{e}_1 = \frac{\mathbf{a}+\mathbf{b}}{|\mathbf{a}+\mathbf{b}|}, \quad \mathbf{e}_2 = \frac{-\mathbf{a}+\mathbf{b}}{|\mathbf{a}+\mathbf{b}|}, \quad \mathbf{e}_3 = \frac{\mathbf{c}}{|\mathbf{c}|}.$$

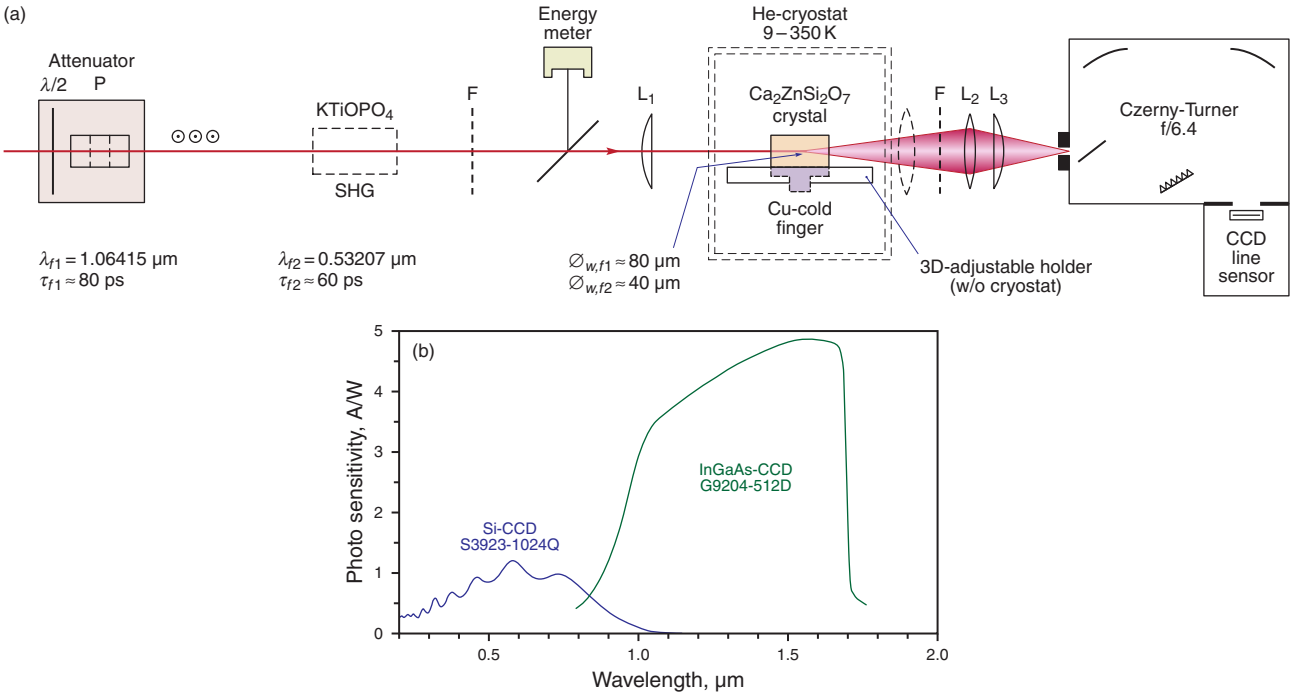

Figure 2 (online color at www.lphys.org) (a) – registration part of the experimental setup. P: polarizer; L1-L3; lenses; F: filter (see also text). (b) – spectral sensitivity of the used Hamamatsu Si- and InGaAs-CCD line sensors (data from Hamamatsu Photonic K.K. technical data sheets)

We also used crystalline samples from a collection of one of the co-authors (A.A.K.). For an estimation of the Raman gain coefficient of the title melilite, YVO_4 was applied as a reference crystal (from China), while for the spectroscopic measurements of spontaneous Raman scattering and in subsidiary SRS-experiments $Ca_2ZnSi_2O_7$ and $Ca_2Ga_2SiO_7$ were used, respectively.

The registration part of our current setup is sketched in Fig. 2a. Into this part output single pulses at $\lambda_{f1} = 1.06415$ μm wavelength, with $\tau_{f1} \approx 80$ ps and the energy up to 40 mJ from a home-made picosecond Nd^{3+}:$Y_3Al_5O_{12}$ mode-locked laser with a double-pass Nd^{3+}:$Y_3Al_5O_{12}$ amplifier are forwarded. After adjustment of the pulse energy by an attenuator a plano-convex lens (L_1) with 250 mm focal length focuses the nearly Gaussian pump beam into the investigated sample, resulting in a beam waist diameter of $\approx$80 μm. The pump beam wavelength can be converted to the SHG ($\lambda_{f2} = 0.53207$ μm) wavelength in a subsequent $KTiOPO_4$ (KTP) crystal leading to a reduced pulse duration of $\tau_{f2} \approx 60$ ps. A Schott BG39 filter glass can be inserted behind the KTP crystal to select the desired pump wavelength. A combination of Schott BG39, BG3, and UG1 filter glasses can be used to spectrally filter the radiation in front of the spectrometer slit. The investigated crystal can be aligned at any angle with respect to the pump beam direction and polarization by a customized three-axis translation and rotation holder. For the cryogenic temperature measurements adjustment of the excitation geometry is restricted to changes of the pump beam polarization. The sample was fixed on the Cu-cold finger in a closed cycle helium cryostat heater combination (Helix CTI cryogenics 8001&8300 controller and compressor, Lakeshore 330 temperature controller). The cold head consists of a two stage refrigeration system (Helix CTI Cryodyne M-22). The temperature is tunable between $\approx$9 K and 350 K. The cryo-chamber size and cooling power are sufficient to investigate sample volumes of several cubic centimeters. At a pump laser repetition rate of 1 Hz heating of the sample is negligible. A spherical, bi-convex lens (L_2) and a cylindrical plano-convex fused silica lens (L_3), both having 100 mm focal length imaged the scattered radiation onto the variable entrance slit of the grating spectrometer in Czerny-Turner arrangement (McPherson Model 270, 6.8 Å/pixel dispersion, 150 lines/mm grating). For the detection of highly divergent emission an additional lens was inserted behind the sample. The spectral components of the collected light are then recorded by a Si-NMOS(CCD) sensor (Hamamatsu S3924-1024Q) for measurements in the UV and visible spectral region, with maximum sensitivity at 0.6 μm, reduced to almost zero around 1.1 μm wavelength (see Fig. 2b). So, for near-IR spectra between 0.9 and 1.7 μm an InGaAs-CMOS(CCD) sensor had to be applied (Hamamatsu G9204-512D).

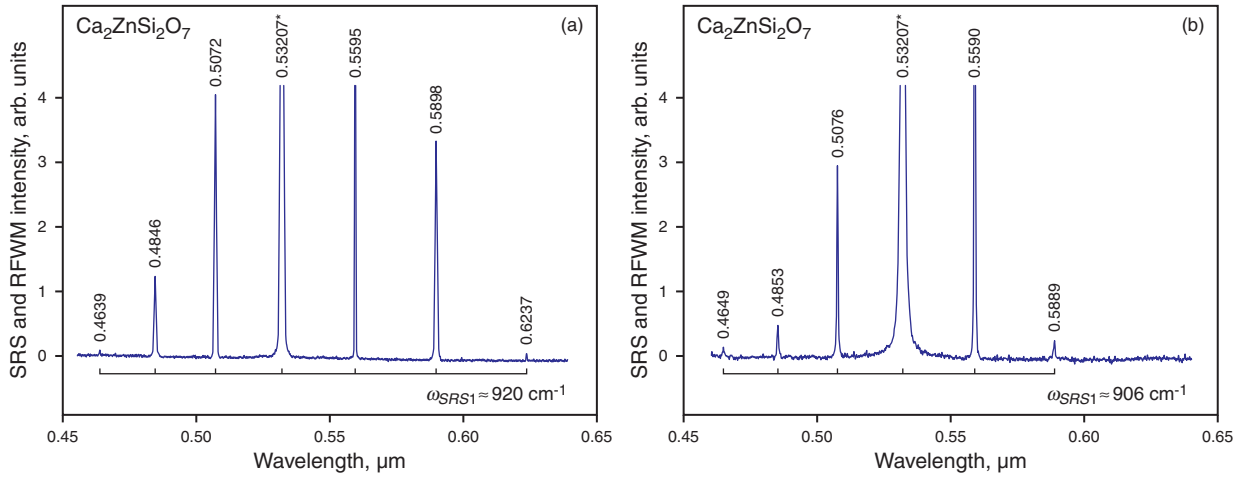

Figure 3 (online color at www.lphys.org) SRS and RFWM spectra of tetragonal $Ca_2ZnSi_2O_7$ crystal, recorded at ≈ 9 K (a) and at ≈ 300 K (b) with picosecond pumping at the wavelength $\lambda_{f2} = 0.53207$ μm in excitation geometry $\mathbf{e}_1[\mathbf{e}_3\mathbf{e}_3]\mathbf{e}_1$ (for definition of $\mathbf{e}_i$ see text). The wavelength of all lines (pump line asterisked) are given in μm, their intensities are shown without correction for the spectral sensitivity of the used multichannel analyzing system with Si-CCD line sensor. The energy spacing (related to the SRS-promoting vibration mode $\omega_{SRS1} \approx 906$ cm^{-1} for ≈ 300 K and $\omega_{SRS1} \approx 920$ cm^{-1} for ≈ 9 K) of the Stokes and anti-Stokes lasing sidebands, is indicated by the horizontal scale brackets. The assignment of all recorded nonlinear lines is given in Table 3 and Table 4

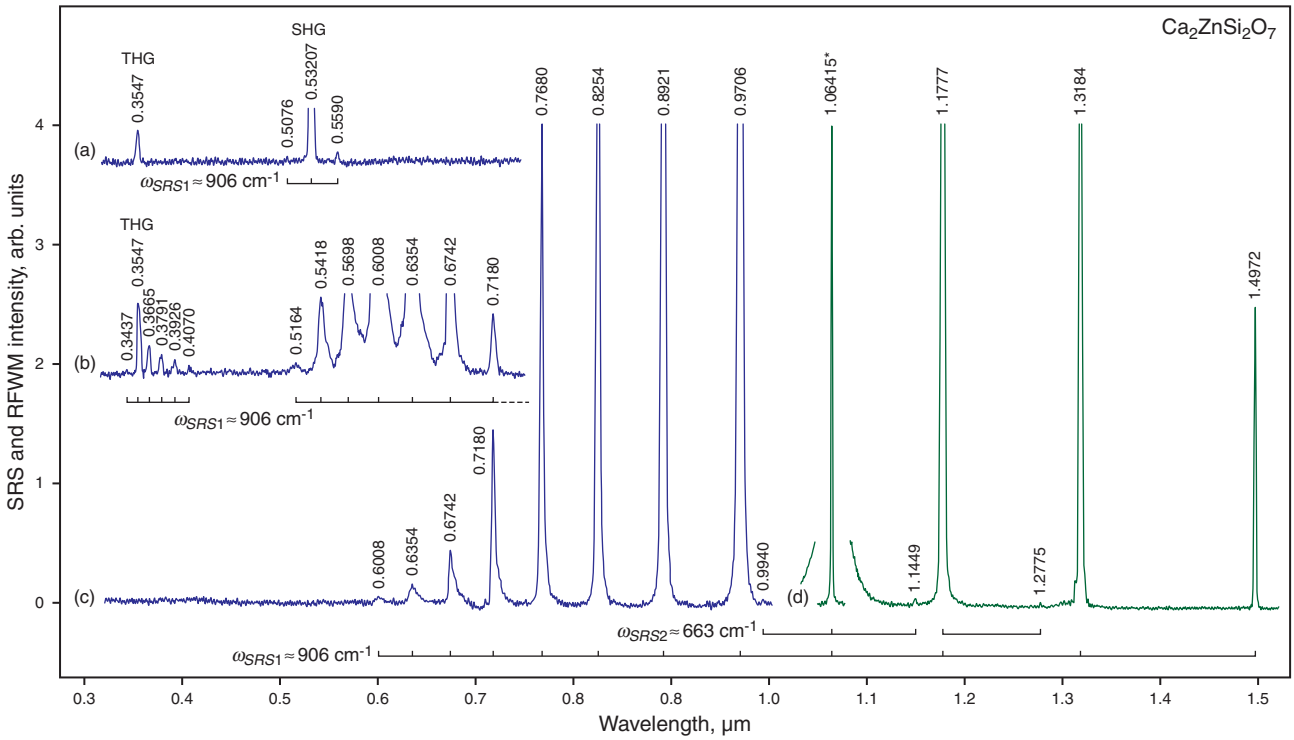

Figure 4 (online color at www.lphys.org) Spectral fragments of SRS and RFWM lasing in tetragonal $Ca_2ZnSi_2O_7$ crystals recorded at room temperature with picosecond pumping at $\lambda_{f1} = 1.06415$ μm wavelength in excitation geometries: (a) $\mathbf{e}_3[\mathbf{e}_1\mathbf{e}_1]\mathbf{e}_3$ and (b)–(d) $\mathbf{e}_1[\mathbf{e}_3\mathbf{e}_3]\mathbf{e}_1$ (for definition of $\mathbf{e}_i$ see text). Fragments (a)–(c) were recorded with a Si-CCD line sensor, fragment (d) with an InGaAs-CCD line sensor. Spacing between lines of $\chi^{(3)}$ nonlinear Stokes and anti-Stokes two-octave lasing comb and multi-wave parametric cascaded ($\chi^{(3)} \rightarrow \chi^{(3)}$) and ($\chi^{(2)} \rightarrow \chi^{(3)}$) generation near the SHG and THG lines is multiple for single SRS-promoting vibration mode $\omega_{SRS1} \approx 906$ cm^{-1} of the studied crystal and is indicated by the horizontal scale brackets. The assignment of all recorded nonlinear lines is given in Table 3. Used notation as in Fig. 3

In the course of our SRS investigations of the crystal of $Ca_2ZnSi_2O_7$ we observed several nonlinear-optical $\chi^{(3)}$- and $\chi^{(2)}$-interactions with picosecond laser excitation at the two fundamental wavelengths $\lambda_{f1} = 1.06415$ μm and $\lambda_{f2} = 0.53207$ μm. These effects comprise sesqui-octave bandwidth (≈ 13592 cm^{-1}) Stokes and anti-Stokes comb generation via SRS and RFWM, non-phase matched SHG and THG, cross-cascaded $\chi^{(3)} \leftrightarrow \chi^{(3)}$ lasing involving different SRS-promoting phonons, as well as several types of cascaded $\chi^{(3)} \leftrightarrow \chi^{(3)}$ and $\chi^{(2)} \leftrightarrow \chi^{(3)}$ self-SFG conversion acts in the spectral regions around the SHG and THG lines. Within these interactions five SRS-phonons appeared, among them three $\omega_{SRS1} \approx 906$ cm^{-1}, $\omega_{SRS2} \approx 663$ cm^{-1}, and $\omega_{SRS3} \approx 614$ cm^{-1} (all at room temperature), and $\omega_{SRS1} \approx 920$ cm^{-1}, $\omega_{SRS2} \approx 670$ cm^{-1}, and $\omega_{SRS3} \approx 620$ cm^{-1} (all at $\approx$9 K), which are directly related to the three strongest lines in spontaneous Raman scattering spectra and two "combined" phonons $\omega_{SRS4} \approx 250$ cm^{-1} and $\omega_{SRS5} \approx 300$ cm^{-1} (all at $\approx$9 K), and $\omega_{SRS4} \approx 243$ cm^{-1} (at room temperature). The latter in no way manifested in the spontaneous Raman spectra at room temperature of the title melilite. At this stage of the study of the $\chi^{(3)}$-nonlinear-laser potential of the $Ca_2ZnSi_2O_7$ crystal we hypothesize that they are the result of an interaction between three "original" phonons as

$$\omega_{SRS1}(\approx 920\ \text{cm}^{-1}) - \omega_{SRS2}(\approx 670\ \text{cm}^{-1}) =$$

$$= \omega_{SRS4}(\approx 250\ \text{cm}^{-1})$$

and

$$\omega_{SRS}(\approx 920\ \text{cm}^{-1}) - \omega_{SRS3}(\approx 620\ \text{cm}^{-1}) =$$

$$= \omega_{SRS5}(\approx 300\ \text{cm}^{-1}).$$

Selected spectra recorded in different excitation geometry at room temperature and at $\approx$9 K and the results of their analysis are shown in Fig. 3 – Fig. 7, and are summarized in Table 3 and Table 4.

As shown by the accumulated knowledge received during SRS-spectroscopy of centrosymmetric and non-centrosymmetric crystals of each of them have individual numerous manifestations of cascaded and cross-cascaded ($\chi^{(3)} \leftrightarrow \chi^{(3)}$)- and ($\chi^{(3)} \leftrightarrow \chi^{(2)}$)-interactions (see, e.g. [29–35]). Even in families of isostructural crystals it is very difficult to find crystals with the same nonlinear-laser properties. As shown in Table 1 and the present study the tetragonal non-centrosymmetric crystals with the melilite-type structure make no exception. Particularly interesting is the discovery of the cascaded (like high-order SRS and RFWM generation related to three original $\chi^{(3)}$-active phonons (see Fig. 3, Fig. 4, Fig. 5a, and Fig. 6) and the cross-cascaded $\chi^{(3)}$-lasing involving both the original and arising two "combined" phonons

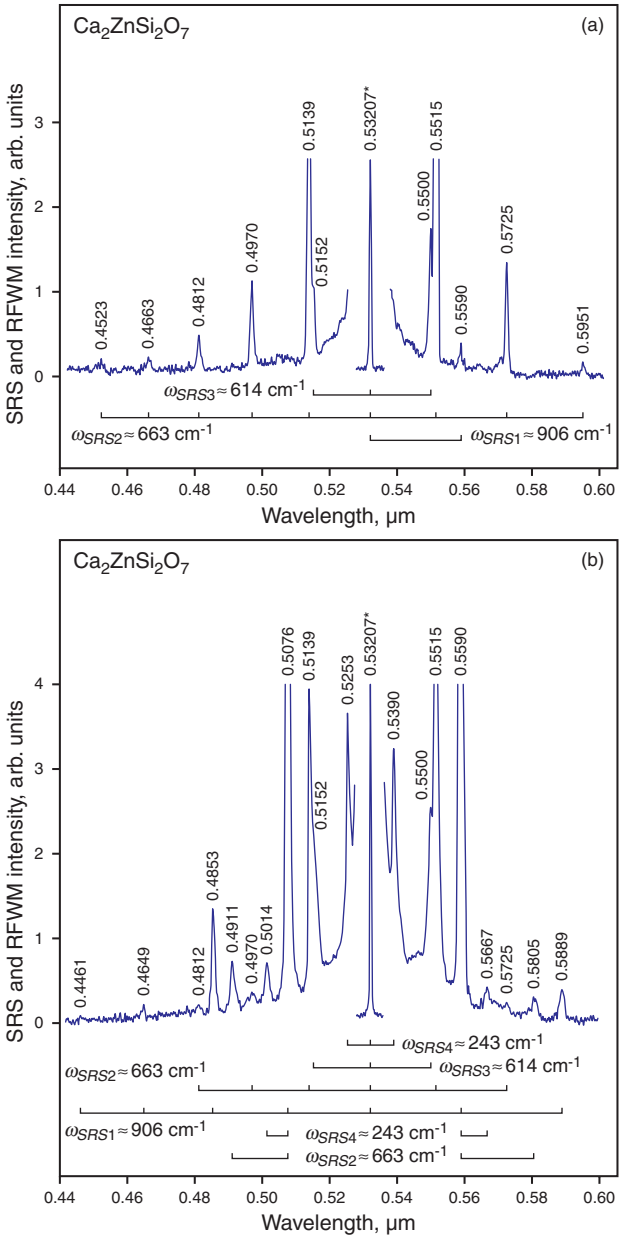

Figure 5 (online color at www.lphys.org) SRS and RFWM spectra of tetragonal $Ca_2ZnSi_2O_7$ crystal, recorded at room temperature with picosecond pumping at the wavelength $\lambda_{f2} = 0.53207$ μm in excitation geometries: (a) $\mathbf{e}_2[(\mathbf{e}_1+\mathbf{e}_3)(\mathbf{e}_1+\mathbf{e}_3)]\mathbf{e}_2$ and (b) $\mathbf{e}_1[(\mathbf{e}_2+\mathbf{e}_3)(\mathbf{e}_2+\mathbf{e}_3)]\mathbf{e}_1$ (for definition of $\mathbf{e}_i$ see text). The wavelength of all lines (pump line asterisked) are given in μm, their intensities are shown without correction for the spectral sensitivity of the used multichannel analyzing system with Si-CCD line sensor. The energy spacing (related to the SRS-promoting vibration modes $\omega_{SRS1} \approx 906$ cm^{-1}, $\omega_{SRS2} \approx 663$ cm^{-1}, and $\omega_{SRS3} \approx 614$ cm^{-1} for the spectrum (a) and $\omega_{SRS1} \approx 906$ cm^{-1}, $\omega_{SRS2} \approx 663$ cm^{-1}, $\omega_{SRS3} \approx 614$ cm^{-1}, and $\omega_{SRS4} \approx 243$ cm^{-1} for the spectrum (b) of the Stokes and anti-Stokes lasing sidebands, is indicated by the horizontal scale brackets. The assignment of all recorded nonlinear lines is given in Table 3. Used notation as in Fig. 3

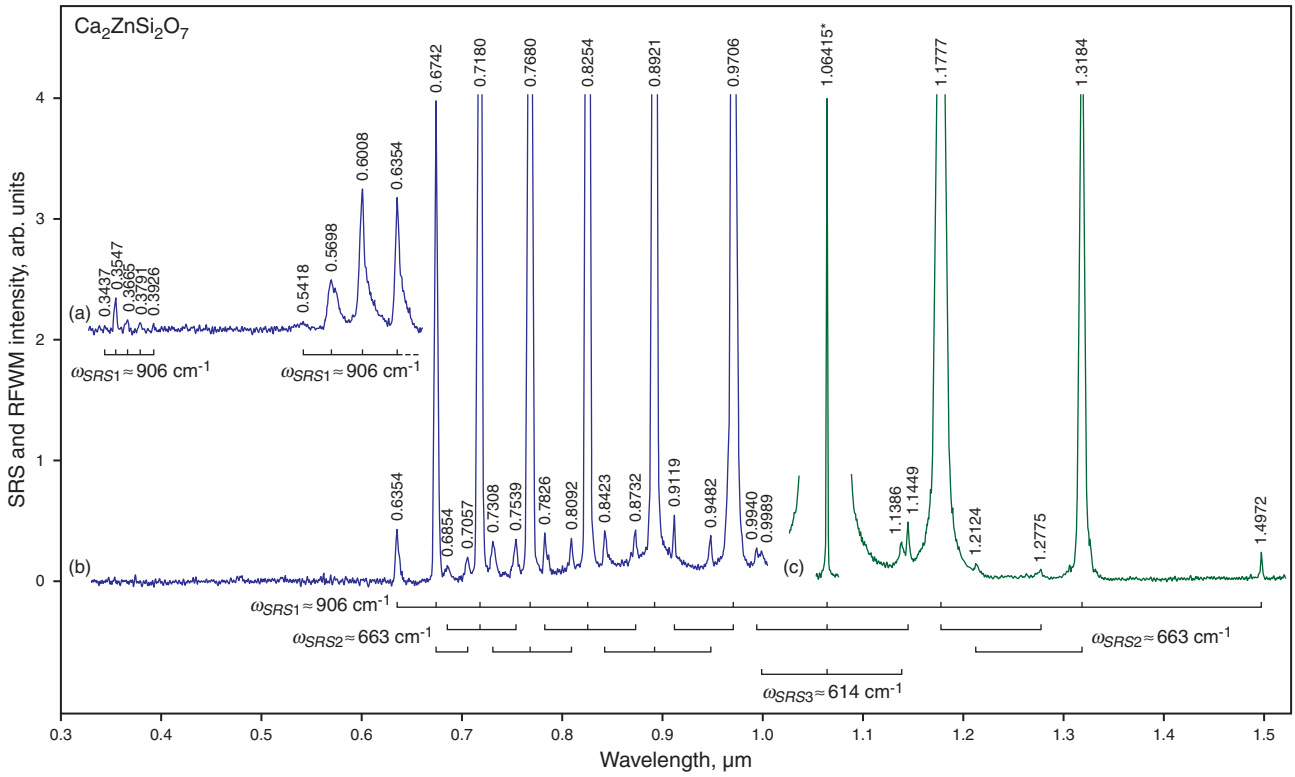

Figure 6 (online color at www.lphys.org) Spectral fragments of SRS and RFWM lasing in tetragonal $Ca_2ZnSi_2O_7$ crystals recorded at room temperature with picosecond pumping at $\lambda_{f1} = 1.06415$ μm wavelength in excitation geometry $\mathbf{e}_2[\mathbf{e}_3\mathbf{e}_3]\mathbf{e}_2$ (for definition of $\mathbf{e}_i$ see text). Fragments (a) and (b) were recorded with a Si-CCD line sensor, fragment (c) with an InGaAs-CCD line sensor. Spacing between lines of $\chi^{(3)}$ nonlinear Stokes and anti-Stokes two-octave lasing comb and multi-wave parametric cascaded ($\chi^{(3)} \rightarrow \chi^{(3)}$) generation is multiple for three SRS-promoting vibration modes $\omega_{SRS1} \approx 906$ cm^{-1}, $\omega_{SRS2} \approx 663$ cm^{-1}, and $\omega_{SRS3} \approx 614$ cm^{-1} of the studied crystal and is indicated by the horizontal scale brackets. The assignment of all recorded nonlinear lines is given in Table 3. Used notation as in Fig. 3

(see Fig. 5b and Fig. 7). The nature of the manifestations of these phonons in the title crystal will be object of special work after the exploratory survey of SRS-properties of several other isostructural melilites. Depending on the geometry at one-micron pumping (at $\lambda_{f1} = 1.06415$ μm or $\omega_{f1} \approx 9397$ cm^{-1}), third harmonic generation ($\lambda_{f3} = 0.3547$ μm or $\omega_{f3} \approx 29191$ cm^{-1}) in non-centrosymmetric $Ca_2ZnSi_2O_7$ crystal can be excited both, by two-frequency ($\omega_{f1} + \omega_{f2} = \omega_{f3}$, see Fig. 4a), and three-frequency ($\omega_{f1} + \omega_{f1} + \omega_{f1} = \omega_{f3}$, see Fig. 4b) parametric interactions. Active cascaded ($\chi^{(3)} \rightarrow \chi^{(3)}$) interactions in the title melilite have allowed us to indirectly register its fourth Stokes generation (at λ_{St4-1}=1.7322 μm, see Table 3) under one-micron pumping via the four-wave parametric process self-SFG $\{\lambda_{f1}, \lambda_{St4-1}\}$ that "transferred" the mid-IR radiation into the ultraviolet region of the spectrum ($\omega_{f1} + \omega_{f1} + \omega_{St4-1} = \omega_{SFG,St4-1} = 24570$ cm^{-1} or $\lambda_{SFG,St4-1} = 0.4070$ μm, see Fig. 4b). In our experiment, recording this fourth Stokes component was not possible due to almost "zero" sensitivity of the used InGaAs-CCD sensor (see Fig. 2b). We believe that our interpretation is correct, although a more reliable result would be given by a direct measurement. The fact that the above four-wave parametric process is not the only one, in principle, there may be other similar processes, but their functional probability is extremely small. We will also explore the tempting possibility of correctly attach the self-SFG lasing components to Stokes and anti-Stokes comb. There is evidence that the "gap" between the parts of the $\chi^{(3)}$-spectrum (21 lasing components, Fig. 4b– Fig. d) should not affect the efficiency of the synthesis process of ultrashort waveforms.

At the present stage of our SRS investigation of the $Ca_2ZnSi_2O_7$ crystal, we have roughly estimated the room-temperature steady-state (ss) Raman gain coefficient ($g_{ssR}^{St_{1-1}}$) only for its first Stokes generation at $\lambda_{St1-1} = 1.1777$ μm wavelength (see Fig. 4d), which is promoted by the most SRS-active vibration mode $\omega_{SRS1} \approx 906$ cm^{-1}. This was possible because our excitation conditions are well suited to the condition $\tau_f \ll T_2 = (\pi \Delta\nu_R)^{-1} \approx 1$ ps (here T_2 and $\Delta\nu_R \approx 11$ cm^{-1}

are the phonon relaxation time and the linewidth of the corresponding SRS-promoting vibration transition, respectively (see Fig. 8)). For this purpose, we used the sufficiently tested method based on the well-known relation $g_{ssR}^{St_{1-1}} I_f^{thr} l_{SRS} \approx 30$ (see. e.g. [36]) in combination with comparative measurements of the "threshold" pump intensity I_f^{thr} (according to the conventional definition adopted in [37, 38]) of the confidently detectable first-Stokes lasing signal for the studied crystal and for a reference crystal. Here, yttrium vanadate (YVO_4) was utilized with a wavelength of the first Stokes component of $\lambda_{St1} = 1.1755$ μm and a rather reliably determined value of $g_{ssR}^{St1} \approx 4.5$ cm/GW [39] under comparable pumping conditions and equal SRS-active length (l_{SRS}). We found that the measured threshold for yttrium vanadate in excitation geometry $c(aa)c$ (details of the experiment see in [39]) was approximately 25 times less than that for $Ca_2ZnSi_2O_7$ crystal in excitation geometry $\mathbf{e}_1[(\mathbf{e}_2+\mathbf{e}_3)(\mathbf{e}_2+\mathbf{e}_3)]\mathbf{e}_1$. This results in a value of the room-temperature steady-state Raman gain coefficient $g_{ssR}^{St_{1-1}}$ for the first Stokes generation of the melilite studied in excitation geometry $\mathbf{e}_1[(\mathbf{e}_2+\mathbf{e}_3)(\mathbf{e}_2+\mathbf{e}_3)]\mathbf{e}_1$ at the wavelength $\lambda_{St1-1} = 1.1777$ μm of not less than 0.2 cm/GW.

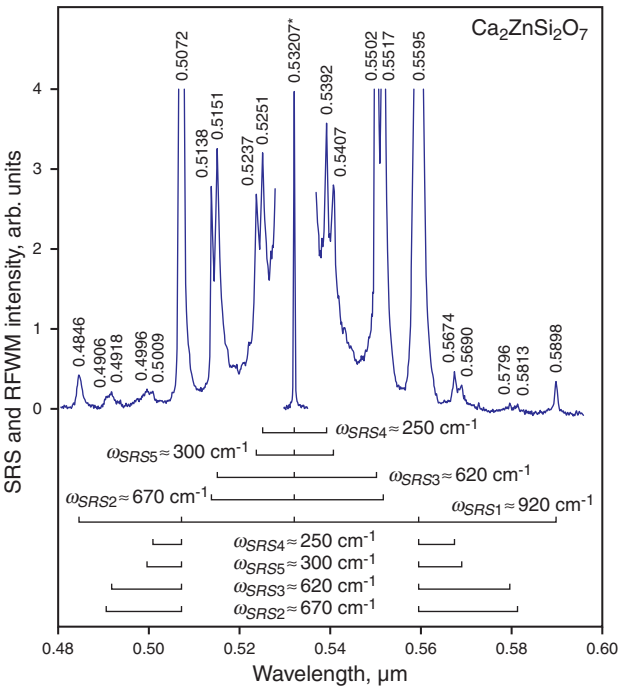

Figure 7 (online color at www.lphys.org) SRS and RFWM spectra of tetragonal $Ca_2ZnSi_2O_7$ crystal, recorded at ≈ 9 K with picosecond pumping at the wavelength $\lambda_{f2} = 0.53207$ μm in excitation geometry $\mathbf{e}_1[(\mathbf{e}_2+\mathbf{e}_3)(\mathbf{e}_2+\mathbf{e}_3)]\mathbf{e}_1$ (for definition of $\mathbf{e}_i$ see text).The wavelength of all lines (pump line asterisked) are given in μm, their intensities are shown without correction for the spectral sensitivity of the used multichannel analyzing system with Si-CCD line sensor. The energy spacing (related to the SRS-promoting vibration mode $\omega_{SRS1} \approx 920$ cm^{-1}, $\omega_{SRS2} \approx 670$ cm^{-1}, $\omega_{SRS3} \approx 620$ cm^{-1}, $\omega_{SRS4} \approx 250$ cm^{-1}, and $\omega_{SRS5} \approx 300$ cm^{-1} of the Stokes and anti-Stokes lasing sidebands, is indicated by the horizontal scale brackets. The assignment of all recorded nonlinear lines is given in Table 4. Used notation as in Fig. 3

3. SRS-promoting phonon modes

As already mentioned above (Table 2) the average structure of two-dimensionally incommensurately modulated $Ca_2ZnSi_2O_7$ crystal (at room temperature) agrees with the melilite-type structure with space group symmetry $D_{2d}^3 - P\bar{4}2_1m$. For factor group analysis [40] of $Ca_2ZnSi_2O_7$ we refer to the average structure. Its primitive cell ($Z = 2$) consists of 4 calcium, 2 zinc, 4 silicium, and 14 oxygen atoms, that occupy the following positions (see, Table 2 and e.g. [18]): 4e-C_s (Ca, Si, and O2), 2a-S_4 (Zn), 2c-C_{2v} (O1), and 8f-C_1 (O3). The D_{2d}^3-tetragonal unit cell of the studied crystal comprises 24 atoms that have 72 zone-center ($\mathbf{k} = 0$) vibrational degrees of freedom distributed among the irreducible representation [38]: $\Gamma_{72} = 10A_1 + 6A_2 + 7B_1 + 11B_2 + 19E$. It could be further subdivided into (see, e.g. [10, 39]): $\Gamma(Ca^{2+}) = 2A_1 + A_2 + B_1 + 2B_2 + 3E$ (translations of calcium atoms with site symmetry C_s), $\Gamma(Zn^{2+}) = B_1 + B_2 + 2E$ (translations of zinc atoms with symmetry S_4), $\Gamma(Si^{4+}) = 2A_1 + A_2 + B_1 + 2B_2 + 3E$ (translations of silicium atoms with site symmetry C_s), $\Gamma(O^{2-}1) = A_1 + B_2 + 2E$, $\Gamma(O^{2-}2) = 2A_1 + A_2 + B_1 + 2B_2 + 3E$, and $\Gamma(O^{2-}3) = 3A_1 + 3A_2 + 3B_1 + 3B_2 + 6E$. Among the 72 possible variations of the crystal lattice of $Ca_2ZnSi_2O_7$ crystal, 69 phonons $\Gamma_O = 10A_1 + 6A_2 + 7B_1 + 10B_2 + 18E$ correspond to the optical modes and three remaining phonons, $\Gamma_T = B_2 + E$ describe the acoustic modes. Since the unit cell of the title crystal contains two Si_2O_7 units, degrees of freedom associated with three oxygen and silicium atoms contribute to internal and lattice modes of these units. The 21 internal modes of a free Si_2O_7 group can be subdivided into symmetric and asymmetric stretching modes of the SiO_3 groups [$\nu_s(SiO_3)$:$A_1 + B_1$] and [$\nu_{as}(SiO_3)$:$A_1 + B_1 + B_2 + A_2$], respectively; symmetric and asymmetric stretching modes of the Si-O-Si bridge [ν_s(SiOSi):A_1] and [ν_{as}(SiOSi):B_1], respectively; bending mode of the Si-O-Si bridge [δ(SiOSi):A_1], rocking modes of the SiO_3 groups [$\tau(SiO_3)$:$A_2 + B_2$], and O-Si-O bending modes [δ(OSiO):$3A_1 + 2A_2 + 3B_1 + 2B_2$] (see, e.g. [41–43]). In the crystal these modes will give rise to $\Gamma_{int} = 7A_1 + 4A_2 + 4B_1 + 7B_2 + 10E$ internal modes. Translational and librational modes of Si_2O_7 units are distributed among $\Gamma'_T = A_1 + B_2 + 2E$ and $\Gamma_L = A_2 + B_1 + 2E$ representation, respectively. A selected spontaneous Raman scattering spectrum of $Ca_2ZnSi_2O_7$ single crystal recorded at room temperature is shown in Fig. 8 and the lists of wavenumbers of its Raman shifted lines

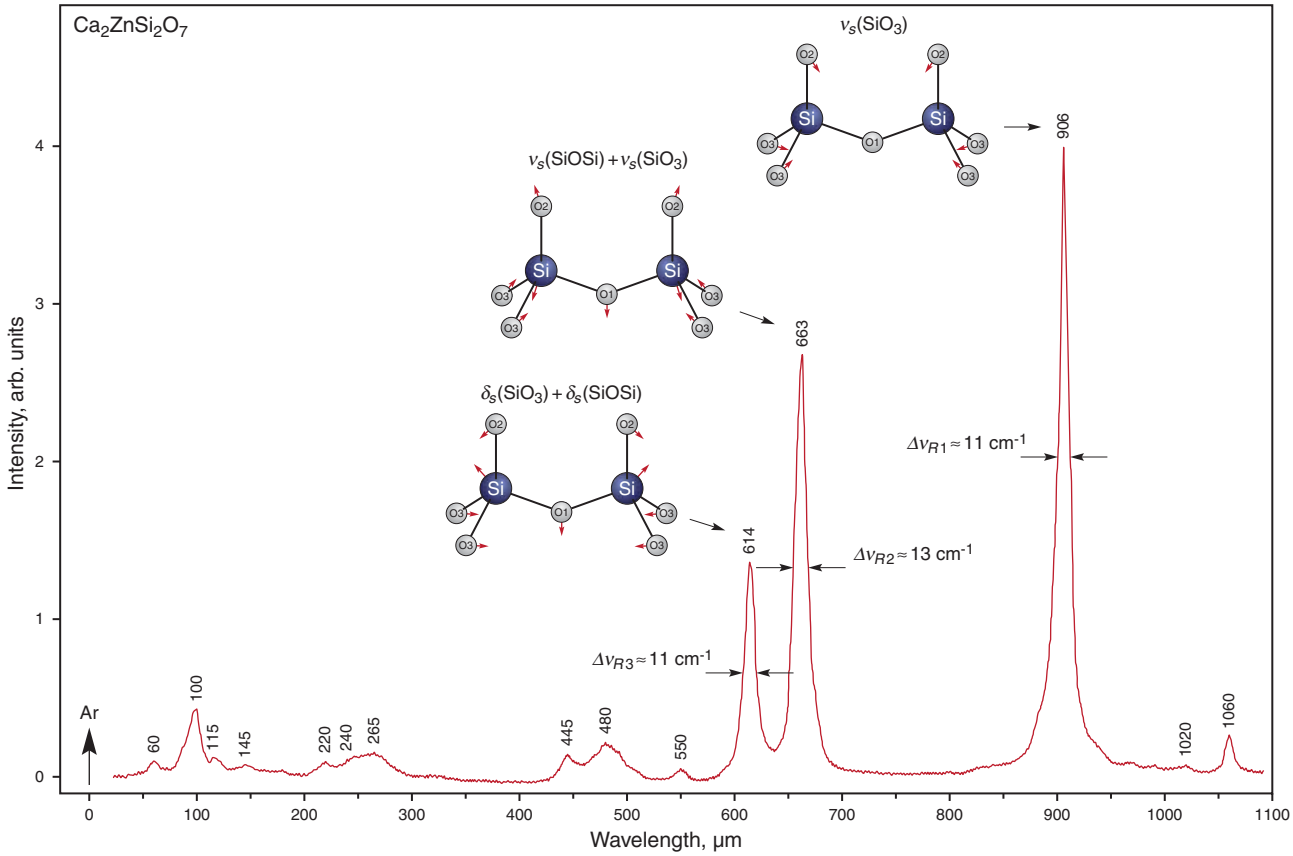

Figure 8 (online color at www.lphys.org) First order spontaneous Raman scattering A_1-spectrum of a $Ca_2ZnSi_2O_7$ single crystal, recorded at room temperature in excitation geometry $\approx b(cc)\approx b$ using a Raman spectrometer Jobin Yvon model T-64000 with Ar-ion laser excitation at 0.5146 μm wavelength (indicated by a vertical arrow). Energy of selected Raman shifted lines is given in cm^{-1} (see also text)

with tentative assignment is given in Table 5. These data suggest that three intense lines from the region 600 – 910 cm^{-1} correspond to the SRS-promoting phonon modes (see Table 3 and Table 4). They have been assigned to the symmetric vibrations of the Si_2O_7 groups. The strongest Raman line at $\approx$ 906 cm^{-1} should be identified with the fully symmetric $\nu_s(SiO_3)$ A_1-mode. Two other intense lines at $\approx$ 664 and $\approx$ 614 cm^{-1} can be assigned to ν_s(SiOSi) and $\delta_s(SiO_3)+\delta_s$(SiOSi) modes, respectively. The atomic displacement vectors for these phonons are sketched as insets of Fig. 8. A detailed analysis of the polarized spontaneous Raman and IR spectra of $Ca_2ZnSi_2O_7$ and other silicate crystals will be published in an upcoming paper.

4. Conclusion

The obtained new knowledge from the conducted experiments with the tetragonal crystal of $Ca_2ZnSi_2O_7$ expanded its functional nonlinear laser potential. At present time, among the few SRS-melilites the $Ca_2ZnSi_2O_7$ crystal exhibits the largest number of $\chi^{(3)}$-promoting vibrations, as well as a manifestation of "combined" modes. The origin of these modes in the regime of SRS-generation as well as their participation in the cross-cascaded $\chi^{(3)}$-lasing processes is of particular interest for nonlinear optics and solid-state physics. To understand this nonlinear-laser phenomenon, we plan to explore other melilite-type crystals. For a detailed study of the manifestations of these modes in $\chi^{(3)}$ generation processes, we have carried out corresponding measurements at cryogenic temperatures (see Fig. 7 and Table 4). All recorded SRS and multi-wave parametric lasing components of the $Ca_2ZnSi_2O_7$ crystal were identified and attributed to its $\chi^{(3)}$-promoting vibration modes. For the case of the first Stokes generation at $\lambda_{St1-1}=1.1777$ μm wavelength related to $\omega_{SRS1}\approx 906$ cm^{-1} under one-micron pumping we roughly estimated the room-temperature steady-state Raman gain coefficient $g_{ssR}^{St_{1-1}}\geq 0.2$ cm/GW of the title crystal. Data presented here together with the results of the study of the four already known SRS-active melilites (see

Table 1 and [9, 11, 12] testify the importance of continued comprehensive studies of optical and nonlinear-laser properties of further crystals with the melilite-type structure.

Acknowledgements The authors wish to note that the investigation was considerably enhanced through mutual scientific help within the "Joint Open Laboratory for Laser Crystal and Precise Laser Systems", and was stimulated by research programs of the Institute of Crystallography of the Russian Academy of Sciences, by the Institute of Optics and Atomic Physics of the Technical University of Berlin, by the Institute of Crystallography of the University of Cologne, by the Institute for Laser Science of the Tokyo University of Electro-Communication, and by the Institute of Low Temperature and Structure Research of the Polish Academy of Sciences. One of us (A.A.K.) is grateful to the Russian Foundation for Basic Research, the Program "Extreme Light Fields and Their Applications" of the Presidium of Russian Academy of Sciences and the Alexander von Humboldt Foundation.

References

[1] M. Alam, K.H. Gooen, B. Di Bartolo, A. Linz, E. Sharp, L. Gillespie, and G. Janney, J. Appl. Phys. **39**, 4728 (1968).
[2] D.J. Horowitz, L.F. Gillespie, J.E. Miller, and E.J. Sharp, J. Appl. Phys. **43**, 3527 (1972).
[3] A.A. Kaminskii, E.L. Belokoneva, B.V. Mill, S.E. Sarkisov, and K. Kurbanov, Phys. Status Solidi (a) **97**, 279 (1986).
[4] W. Ryba-Romanowski, B. Jeżowska-Trzebiatowska, W. Piekarczyk, and M. Berkowski, J. Phys. Chem. Solids **49**, 199 (1988).
[5] T.H. Allik, M.J. Ferry, R.J. Reeves, R.C. Powell, W.W. Hovis, D.P. Caffey, R.A. Utano, L. Merkle, and C.F. Campana, J. Opt. Soc. Am. B **7**, 1190 (1990).
[6] F. Hanson, D. Dick, H.R. Verdun, and M. Kokta, J. Opt. Soc. Am. B **8**, 1668 (1991).
[7] I. Pracka, W. Giersz, M. Świrkowicz, A. Pajaczkowska, S. Kaczmarek, Z. Mierczyk, and K. Kopczyński, Mater. Sci. Eng. B **26**, 201 (1994).
[8] A.A. Kaminskii, H. Nakao, L. Bohatý, P. Becker, J. Liebertz, R. Kleinschrodt, K. Ueda, and A. Shirakawa, Laser Phys. Lett. **7**, 876 (2010).
[9] A.A. Kaminskii, L. Bohatý, P. Becker, J. Liebertz, P. Held, H.J. Eichler, H. Rhee, and J. Hanuza, Laser Phys. Lett. **5**, 845 (2008).
[10] J. Hanuza, M. Maçzka, M. Ptak, J. Lorenc, K. Hermanowicz, P. Becker, L. Bohatý, and A.A. Kaminskii, J. Raman Spectrosc. **42**, 782 (2011).
[11] P. Becker, L. Bohatý, J. Liebertz, H.-J. Kleebe, M. Müller, H.J. Eichler, H. Rhee, J. Hanuza, and A.A. Kaminskii, Laser Phys. Lett. **7**, 367 (2010).
[12] A.A. Kaminskii, L. Bohatý, P. Becker, J. Liebertz, H.J. Eichler, H. Rhee, and J. Hanuza, Laser Phys. Lett. **7**, 528 (2010).
[13] A.A. Kaminskii, E.L. Belokoneva, B.V. Mill', S.A. Tamazyan, and K. Kurbanov, Inorg. Mater. **22**, 993 (1986).
[14] A.A. Kaminskii, H.E. Verdun, and B.V. Mill, Phys. Status Solidi (a) **129**, K125 (1992).
[15] A.A. Kaminskiĭ, V.A. Karasev, V.D. Dubrov, V.P. Yakunin, B.V. Mill', and A.V. Butashin, Sov. J. Quantum Electron. **22**, 97 (1992).
[16] L. Bindi, M. Czank, F. Röthlisberger, and P. Bonazzi, Am. Mineral. **86**, 747 (2001).
[17] Z.H. Jia, W. Massa, W. Treutmann, A.K. Schaper, and H. Rager, Acta Cryst. B **62**, 547 (2006).
[18] S.J. Louisnathan, Z. Kristallogr. **130**, 427 (1969).
[19] L. Bohatý and J. Liebertz, Z. Kristallogr. **159**, 277 (1982).
[20] E.R. Segnit, J. Am. Ceram. Soc. **37**, 273 (1954).
[21] J. Liebertz and S. Stähr, Z. Kristallogr. **159**, 271 (1982).
[22] B. Bagautdinov, K. Hagiya, S. Noguchi, M. Ohmasa, N. Ikeda, K. Kusaka, and K. Iishi, Phys. Chem. Miner. **29**, 346 (2002).
[23] S. Haussühl and J. Liebertz, Phys. Chem. Miner. **31**, 565 (2004).
[24] S.L. Webb, C.R. Ross, and J. Liebertz, Phys. Chem. Miner. **18**, 522 (1992).
[25] O. Medenbach and R.D. Shannon, J. Opt. Soc. Am. B **14**, 3299 (1997).
[26] K. Iishi, T. Mizota, K. Fujino, and Y. Furukawa, Phys. Chem. Miner. **17**, 720 (1991).
[27] S. Haussühl, E. Haussühl, and J. Liebertz, Z. Kristallogr. (Suppl.) **24**, 30 (2006).
[28] T.C. Damen, S.P.S. Porto, and B. Tell, Phys. Rev. **142**, 570 (1966).
[29] A.A. Kaminskii, L. Bohatý, P. Becker, H.J. Eichler, J. Hanuza, M. Maczka, K. Ueda, K. Takaichi, H. Rhee, and G.M.A. Gad, Phys. Status Solidi (a) **201**, 3200 (2004).
[30] A.A. Kaminskii, L. Bohatý, P. Becker, J. Liebertz, H.J. Eichler, and H. Rhee, Laser Phys. Lett. **3**, 519 (2006).
[31] A.A. Kaminskii, L. Bohatý, P. Becker, H.J. Eichler, and H. Rhee, Laser Phys. Lett. **7**, 142 (2010).
[32] A.A. Kaminskii, L. Bohatý, P. Becker, H.J. Eichler, H. Rhee, and J. Hanuza, Laser Phys. Lett. **6**, 872 (2009).
[33] A.A. Kaminskii, S.N. Bagayev, V.V. Dolbinina, A.E. Voloshin, H. Rhee, H.J. Eichler, and J. Hanuza, Laser Phys. Lett. **6**, 544 (2009).
[34] A.A. Kaminskii, Laser Photon. Rev. **1**, 93 (2007).
[35] A.A. Kaminskii, L. Bohatý, P. Becker, H.J. Eichler, and H. Rhee, Phys.-Usp. **51**, 899 (2008).
[36] Y.R. Shen, The Principles of Nonlinear Optics (Wiley, New York, 1984).
[37] K.K. Lai, W. Schüsslbauer, H. Silberbauer, H. Amler, U. Bogner, M. Maier, M. Jordan, and H.-J. Jodl, Phys. Rev. B **42**, 5834 (1990).
[38] A.A. Kaminskii, P. Becker, L. Bohatý, K. Ueda, K. Takaichi, J. Hanuza, M. Maczka, H.J. Eichler, and G.M.A. Gad, Opt. Commun. **206**, 179 (2002).
[39] A.A. Kaminskii, K. Ueda, H.J. Eichler, Y. Kuwano, H. Kouta, S.N. Bagaev, T.H. Chyba, J.C. Barnes, G.M.A. Gad, T. Murai, and J.R. Lu, Opt. Commun. **194**, 201 (2001).
[40] D.L. Rousseau, R.P. Bauman, and S.P.S. Porto, J. Raman Spectrosc. **10**, 253 (1981).
[41] A.N. Lazarev, Vibrational Spectra and Structure of Silicates (Consultants Bureau, Plenum, New York, 1972).
[42] S.K. Sharma, H.S. Yoder, Jr., and D.W Matson, Geochim. Cosmochim. Acta **52**, 1961 (1988).
[43] U. Kuhlmann, C. Thomsen, A.V. Prokofiev, F. Büllesfeld, E. Uhrig, and W. Assmus, Physica B **301**, 276 (2001).